**Revision 2**

# Using mineral geochemistry to decipher slab, mantle, and crustal input in the generation of high-Mg andesites and basaltic andesites from the northern Cascade Arc

MAY SAS[1, 2,]*, SUSAN M. DEBARI[2], MICHAEL A. CLYNNE[3], BRIAN G. RUSK[2]

[1]University of Auckland School of Environment, Private Bag 92019, Auckland 1142, New Zealand

[2]Western Washington University Geology Department, 516 High Street MS 9080, Bellingham, Washington 98225, U.S.A.

[2]U.S. Geological Survey Volcano Science Center, 345 Middlefield Road MS 910, Menlo Park, California 94025, U.S.A.

*E-mail: msas481@aucklanduni.ac.nz

## ABSTRACT

To better understand the role of slab melt in the petrogenesis of North Cascades magmas, this study focuses on petrogenesis of high-Mg lavas from the two northernmost active volcanoes in Washington. High-Mg andesites (HMA) and basaltic andesites (HMBA) in the Cascade Arc have high Mg# (molar Mg/(Mg+ $Fe^{2+}$)) relative to their $SiO_2$ contents, elevated Nd/Yb, and are Ni- and Cr-enriched. The rock units examined here include the Tarn Plateau HMBA (51.8–54.0 wt% $SiO_2$, Mg# 68–70) and Glacier Creek HMA (58.3–58.7 wt% $SiO_2$, Mg# 63–64) from the Mount Baker Volcanic Field, and the Lightning Creek HMBA (54.8–54.6 $SiO_2$, Mg# 69–73) from Glacier Peak. This study combines major and trace element compositions of minerals and whole rocks to test several petrogenetic hypotheses, and determine which, if any, are applicable to North Cascades HMA and HMBA. In the Tarn Plateau HMBA, rare earth element (REE) equilibrium liquids calculated from clinopyroxene compositions have high Nd/Yb that positively correlate with Mg#. This correlation suggests an origin similar to that proposed for Aleutian adakites, where intermediate, high Nd/Yb slab-derived melts interact with the overlying mantle to become Mg-rich, and subsequently mix with low Nd/Yb, mantle-derived mafic magmas with lower Mg#. In the Glacier Creek HMA, elevated whole rock MgO and $SiO_2$ contents resulted from accumulation of xenocrystic olivine and differentiation processes, respectively, but the cause of high Nd/Yb is less clear. However, high whole rock Sr/P (fluid mobile/fluid immobile) values indicate a mantle source that was fluxed by an enriched, hydrous slab component, likely producing the observed high Nd/Yb REE signature. The Lightning Creek HMBA is a hybridized rock unit with at least three identifiable magmatic components, but only one of which has HMA

characteristics. Cr and Mg contents in Cr-spinel and olivine pairs in this HMA component suggest that its source is a strongly depleted mantle, and high whole rock Sr/P values indicate mantle melting that was induced through hydration, likely adding the component responsible for the observed high Nd/Yb REE pattern. The elevated $SiO_2$ contents (54.6 wt%) of the HMA component resulted from differentiation or high degrees of partial melting of ultramafic material through the addition of $H_2O$. Therefore the Lightning Creek HMBA is interpreted to have originated from a refractory mantle source that underwent melting through interaction with an enriched slab component. Our results indicate that in addition to slab-derived fluids, slab-derived melts also have an important role in the production of HMA and HMBA in the north Cascade Arc.

**Keywords:** High-Mg andesites, slab melt, clinopyroxene REE, Mount Baker, Glacier Peak

## INTRODUCTION

Mount Baker and Glacier Peak are the northernmost active volcanoes in the western United States. They are part of the Cascade volcanic arc that extends from northern California to southern British Columbia (Figure 1). Because the subducting oceanic plate below North America is young (approximately 10 Ma at the trench; Green and Harry 1999), the Cascade Arc is considered a "hot" subduction zone (905 ± 50°C beneath the North Cascades; Syracuse et al. 2010). Consequently, slab melting is feasible in the Cascade Arc (Leeman et al. 2004, 2005; Grove et al. 2005; Ruscitto et al. 2011), and studies involving magnesium-rich andesites from southern Cascade Arc volcanoes (e.g. Lassen region and Mount Shasta) have shown that slab fluids and melts clearly influence magma compositions (Borg et al. 2002; Grove et al. 2002; Walowski et al. 2015, 2016). Overview studies examining magma origin and processes in the northernmost part of the arc, the Garibaldi Volcanic Belt, suggest a decreased contribution from the subducting slab northward along strike with nominal inputs at Mount Meager (Green 2006; Mullen and Weis 2013, 2015). Of the five major the Garibaldi Volcanic Belt volcanic centers only the Mount Baker Volcanic Field, herein referred to as Mount Baker, received detailed attention on multiple lava types erupted through time. Studies involving Mount Baker magnesium-rich lavas conclude mafic magma generation occurs through partial mantle melting and fractionation (Baggerman and DeBari 2011; Moore and DeBari 2012), and a recent study advocates for slab (metabasalt + sediment) melt involvement (Mullen and McCallum 2014).

Magnesian andesites or high-Mg andesites (HMA) are characterized by high Mg# (molar $Mg/(Mg+Fe^{2+})$) relative to their $SiO_2$ concentrations, and are often used as inclusive

terms for the few types of magnesium-rich basalts through dacites, most notably adakites and boninites (Kay 1978; Crawford et al. 1989; Defant and Drummond 1990; Yogodzinski et al. 1995; Stern and Kilian 1996; Calmus et al. 2003; Cooper et al. 2010). Adakites have a steep rare earth element (REE) pattern, due to heavy REE (HREE) depletion, light REE (LREE) enrichment, or both. Adakites are also Sr-enriched (>1000 ppm is common; Yogodzinski and Kelemen 1998; Martin et al. 2005), and their origin is often attributed to partial melting of subducted oceanic crust (Kay 1978; Defant and Drummond 1990; Yogodzinski et al. 2001; Kelemen et al. 2003; Tatsumi and Hanyu 2003; Tatsumi et al. 2003). Boninites are characterized by low $TiO_2$ contents (< 0.5 wt%) and high field strength elements (HFSE) depletion, and are associated with shallow (< 50 km) hydrous melting of depleted mantle in supra-subduction or rift settings (Crawford et al. 1989; Kim and Jacobi 2002; Falloon et al. 2008). In this study we use HMA to reference high-Mg andesites and basaltic andesites (HMBA) from the Cascade Arc that have affinities to primitive adakites. These HMA and HMBA are rich in Cr and Ni and contain mafic minerals in equilibrium with mantle rocks (Clynne and Borg 1997; Yogodzinski et al. 2001; Taylor 2001; Grove et al. 2002; Baggerman and DeBari 2011; Moore and DeBari 2012; Mullen and McCallum 2014).

Though volumetrically sparse, HMA are found in arc setting worldwide and studies examining their origin are essential to understanding magma-generating processes (Defant and Drummond 1990; Stern and Kilian 1996; Calmus et al. 2003; Tatsumi et al. 2003). Proposed HMA origins include (1) mixing between Mg-rich, high Sr and high Nd/Yb slab melts and mantle-derived basalt (Yogodzinski and Kelemen 1998, 2007; Yogodzinski et al. 2001; Kelemen et al. 2003); (2) mixing between silicic melts of strongly metasomatized

mantle and mafic melts of moderately metasomatized to unmetasomatized mantle (Straub et al. 2008, 2011); (3) melting of a strongly depleted mantle fluxed by a hydrous (± melt) slab component (Kushiro 1969; Clynne 1993; Borg et al. 1997; Clynne and Borg 1997; Grove et al. 2002, 2005); (4) fractionation of garnet from mantle-derived basaltic melts, without significant slab input (Macpherson et al. 2006); (5) crustal processes including mixing between dacitic crustal melts and a high-Mg basaltic liquid, melting-assimilation-storage-homogenization (MASH), and assimilation-fractional-crystallization (AFC; Streck et al. 2007; Stern and Kilian 1996; Richards and Kerrich 2007; Chiaradia et al. 2009).

Here we investigate rare HMA and HMBA from Mount Baker and Glacier Peak in the northern Cascade Arc, and constrain the influence of the subducting slab on their origin through analyses of new mineral geochemical data combined with existing whole rock data. In particular, clinopyroxene REE compositions and their associated calculated equilibrium liquids provide a powerful tool to constrain mantle versus slab or crustal inputs to magma generation. From Mount Baker, the Tarn Plateau HMBA and the Glacier Creek HMA were investigated. Mullen and McCallum (2014) also discuss Cathedral Crag as a Mount Baker HMBA, but in a previous study by Moore and DeBari (2012) only a single Cathedral Crag sample exhibits high Mg# relative to $SiO_2$, which the authors attribute to olivine accumulation. Samples from this rock unit also contained heterogeneous mineral assemblages indicative of extensive crustal involvement. Therefore this rock unit was not investigated here. From Glacier Peak, the Lightning Creek HMBA was investigated. Though this rock unit also contains andesitic samples (>57 $SiO_2$ wt%), DeBari et al. (in review) show that the Lightning Creek HMA is a mixing product between the Lightning Creek HMBA and

crustally-derived Glacier Peak dacitic magma. Therefore this study focuses on the origin of the more primitive (~55–57 wt% $SiO_2$) Lightning Creek samples.

## GEOLOGIC SETTING

The Cascade Arc extends over 1,200 km from Lassen Peak in California to Mount Meager in Canada, and volcanism is associated with subduction of the Juan de Fuca Plate beneath the North American Plate at a rate of 45 mm/year in the northern segment (Wilson 1993; McCrory et al. 2006, 2012; Figure 1). Subduction conditions in the northern Cascade Arc include a slab dip of 22°, overlying crustal thickness of 35 km, subduction of an approximately 0.4 km thick sediment package (Syracuse et al. 2010), and thrust temperatures upwards of 200°C at the trench (Oleskevich et al. 1999). The age of the Juan de Fuca Plate beneath Mount Baker and Glacier Peak is interpreted to be roughly 20 Ma (Green and Harry 1999).

Mount Baker (3,286 m) is an active, primarily andesitic stratovolcano that is part of a 1.3 million year old volcanic field (Hildreth et al. 2003). The Tarn Plateau HMBA is a clinopyroxene-rich flow with lesser plagioclase, olivine, and orthopyroxene (Table 1). The Tarn Plateau HMBA outcrop is an erosional remnant of a flow that is ~170 m thick, ~500 m long and located on the southern flanks of Mount Baker (Supplementary Materials Figure 1). The Tarn Plateau HMBA has a K-Ar age of 203 ± 25 ka (Hildreth et al. 2003). The Glacier Creek HMA is plagioclase-rich with lesser clinopyroxene, orthopyroxene, and olivine (Table 1). Several discontinuous outcrops of this rock unit are present along the northwestern slope of Mount Baker in Glacier Creek canyon (Supplementary Materials Figure 1). This rock unit has a K-Ar age of 14 ± 9 ka (Hildreth et al. 2003).

Glacier Peak (3,213 m) is a dominantly dacitic stratovolcano located roughly 90 km southeast of Mount Baker (Figure 1). The Lightning Creek HMBA is plagioclase-rich with lesser clinopyroxene, olivine, and orthopyroxene (Table 1). The columnar jointed outcrop is ~400 m in length and is located 10 km southeast of Glacier Peak's summit (Supplementary Materials Figure 2). Based on known Glacier Peak eruptive activity and evidence for glacial interaction during emplacement, the Lightning Creek unit has been interpreted to be Pleistocene in age, but the absolute age remains unknown (Tabor and Crowder 1969).

## ANALYTICAL METHODS

A total of 11 samples, out of 23 previously analyzed for whole rock composition (Taylor 2001; Baggerman and DeBari 2011; Moore and DeBari 2012), were selected for this study based on their $SiO_2$ content and Mg# (with FeO = 0.80*$FeO_T$ for Mount Baker and 0.85*$FeO_T$ for Glacier Peak; Shaw 2011; Moore and DeBari 2012). Major and minor element concentrations were determined for olivine, clinopyroxene, plagioclase, Cr-spinels, and Fe-Ti oxides (Supplementary Materials Tables 1–4) at the University of Washington using a JEOL 733 Superprobe electron microprobe (EMP) with four wavelength dispersive spectrometers (WDS) and one energy dispersive spectrometer (EDS). Standards were an array of natural and synthetic minerals and glasses. A 15 kV accelerating voltage was used for all minerals. Beam conditions were 15 nA current and < 1 μm diameter spot size for olivine, pyroxene, and oxides, and 10 nA current and 3 μm diameter spot size for plagioclase. Element peak counts were 20–40 s, or the length of time required to obtain a statistical error of 0.4%. Analytical error is < 3% for major elements and < 17% for minor elements. The CITZAF correction method of Armstrong (1988a, 1988b) was applied to the data. Qualitative energy

dispersive X-ray spectroscopy (EDS) analyses of additional Tarn Plateau plagioclase and Lightning Creek clinopyroxene and olivine were done using an EDAX Genesis 2000 attached to a Tescan Vega 5136MM SEM at Western Washington University (Supplementary Materials Table 5). Accelerating voltage was 15 kV and current was 50–55 µA. For EDS data to be compared to EMP data, EMP analyses were used as calibration standards. This was done by reanalyzing EMP spots using EDS and calculating the difference between the two analyses. The differences were averaged and used to correct EDS analyses. Reanalysis and data corrections were done for every sample to obtain the best results. Qualitative EDS data were not used in models or to calculate any crystallization parameters.

Trace element concentrations in clinopyroxene (Table 2) were obtained at Western Washington University using an Agilent 7500ce Quadrupole inductively-coupled plasma-mass spectrometer (ICP-MS) coupled with a NewWave UP213nm laser ablation (LA) system. Clinopyroxene grains were 0.5–2.0 mm in length and ablation spots were dominantly 55 µm in diameter, with a few 40 µm diameter rim analyses. All analyses were done with a repetition rate of 10 Hz and fluence of approximately 15 J/cm$^3$. Helium was used as the carrier gas to transport ablated material and was mixed with Ar prior to entering the ICP-MS torch. Ablation sites were chosen using transmitted light microscopy to avoid accidental analysis of inclusions, and backscattered electron (BSE) imaging and EDS analyses were used to identify specific growth zones. NIST 610 glass was the external standard used, with element concentrations from Jochum et al. (2011). Data reduction was carried out using SILLS (Guillong et al. 2008) with equations from Longerich et al. (1996). Analyzed trace isotopes and their respective typical detection limits at 55 µm include $^{88}$Sr (0.035 ppm), $^{139}$La

(0.025 ppm), $^{140}$Ce (0.027 ppm), $^{141}$Pr (0.022 ppm), $^{146}$Nd (0.128 ppm), $^{147}$Sm (0.150 ppm), $^{153}$Eu (0.041 ppm), $^{157}$Gd (0.138 ppm), $^{159}$Tb (0.022 ppm), $^{163}$Dy (0.091 ppm), $^{165}$Ho (0.024 ppm), $^{166}$Er (0.067 ppm), $^{169}$Tm (0.022 ppm), $^{172}$Yb (0.105 ppm), $^{175}$Lu (0.022 ppm). Additional elements, such as P, Zr, Sn, Pb, and U, were also analyzed to monitor for the accidental analysis of inclusions. All LA-ICP-MS spots were located on previously acquired microprobe spots, and $SiO_2$ contents acquired via EMP were used as an internal standard (specific per spot with 0.39 wt% average LA-ICP-MS detection limits).

Three new whole rock samples were analyzed for major and trace element chemistry (Table 3) at the Washington State University GeoAnalytical Laboratory. These samples represent three distinct mingled magmas observed in a single Lightning Creek sample (Supplementary Materials Figure 3). Major element oxides and trace element concentrations were determined by X-ray fluorescence (XRF) analyses using a ThermoARL Advant'XP + sequential XRF spectrometer. Additional trace element concentrations were determined using an Agilent 7700 ICP-MS. Analytical error is < 3% for major elements and < 9% for trace elements. XRF and ICP-MS sample preparation followed the methods described in Knaack et al. (1994) and Johnson et al. (1999).

One Glacier Creek sample was analyzed for Sr, Nd, and Pb isotopes using a VG Sector 54 thermal ionization mass spectrometer (TIMS) and a Nu plasma multi-collector (MC) ICP-MS at the University of Washington (Table 4). Sr and Nd separations were done in accordance with Nelson (1995), and analytical procedures are fully described in Gaffney et al. (2007), Harkins et al. (2008), and Brach-Papa et al. (2009). The following values were used to normalize measured isotopic ratios, NBS 987 for $^{87}$Sr/$^{86}$Sr (0.710240), La Jolla for

$^{143}Nd/^{144}Nd$ (0.511843), and NIST-981 for $^{208}Pb/^{204}Pb$ (36.721), $^{207}Pb/^{204}Pb$ (15.491), and $^{206}Pb/^{204}Pb$ (16.937). Long term reproducibility (at 2σ) is ± 0.000040 for Sr, ± 0.000030 for Nd, ± 0.000125 for $^{206/204}Pb$, ± 0.000150 for $^{207/204}Pb$, and ± 0.000200 for $^{208/204}Pb$.

## RESULTS

### Petrography and Mineral Compositions

All three rock units are porphyritic with 20–35% phenocrysts. Phenocryst assemblages are clinopyroxene and plagioclase dominant with variable amounts of olivine and orthopyroxene. Mineral populations were determined using textures, zoning trends, core compositions (Mg#, Fo, An), and, for clinopyroxene, trace element abundances. Compositional and textural mineral population variations are summarized in Table 1. Olivine, pyroxene, and plagioclase major and minor element analyses are presented in Figures 2–4 and Supplementary Materials Tables 1–3, respectively. Photomicrographs of textural features are shown in Supplementary Materials Figure 4.

**Tarn Plateau.** The Tarn Plateau basaltic andesite contains 30–35% phenocrysts in hypocrystalline groundmass (Table 1). Clinopyroxene (40–65% of phenocrysts) is euhedral to subhedral and 0.25–3.0 mm in size. Compositions are divisible into two Mg# populations, high Mg# (88–94) cores with normal and reverse zoning in the rims, and low Mg# (73–79) cores with reversely zoned rims. Clinopyroxene Cr contents (140–4500 ppm) are positively correlated with Mg#. Plagioclase (25–45%) is euhedral to anhedral and 0.25–5.0 mm in size. Plagioclase core compositions consist of a coarsely sieved, high An (83–88) group and a finely sieved, mid An (54–58) group. Olivine (10–20%) is euhedral to anhedral, up to 3.0

mm in size, and comprises a mid Fo (84–85) cores group and a low Fo (78–81) cores group. Core Fo contents do not correlate with whole rock Mg# or olivine core Ni contents (800–1600 ppm; Figure 5). Olivine with mid Fo contains Cr-spinel inclusions with Cr# 47– 57 (molar Cr/(Cr+Al)) and Mg# 31–35, and olivine with low Fo contains Cr-spinel inclusions with Cr# 50–66 and Mg# 21–38. Mullen and McCallum (2014) conclude a single Tarn Plateau olivine population despite compositional variations. Orthopyroxene (< 3%) is sparse, subhedral, 0.5–1.0 mm in size, and has Mg# 68–70 cores. Mullen and McCallum (2014) also identified a remnant, mantle-equilibrium orthopyroxene xenocryst ($Wo_2En_{92}Fs_6$) with high Al contents that is present as an inclusion in clinopyroxene. The groundmass consists of glass, ilmenite, titanomagnetite, microlitic plagioclase, pyroxene granules, and iddingsite.

**Glacier Creek.** The andesite of Glacier Creek contains 20–25% phenocrysts in a hypocrystalline groundmass (Table 1). Plagioclase (50–70% of phenocrysts) is euhedral to anhedral and 0.5–4.0 mm in size with an unsieved to coarsely sieved population and a finely sieved population. There is no apparent correlation between textures and core An contents, which overlap between the two populations (43–58 and 43–54, respectively). Clinopyroxene (10–23%) is euhedral to anhedral, 0.25–2.0 mm in size, with Mg# 76–80 and 70–490 ppm Cr cores, and reversely zoned rims. Mg# and Cr contents in clinopyroxene show no correlation in analyzed cores and a positive correlation in analyzed rims. Orthopyroxene (10-20%) is euhedral to subhedral, up to 1.5 mm in size, and has Mg# 70–73 cores. Olivine (3–7%) is subhedral to anhedral and 0.5–2.0 mm in size. Olivine cores are $Fo_{72\text{-}86}$ with high Ni contents (1700–4100 ppm; Figure 5) and represent a single population (see Discussion). Cr-spinel

inclusions are abundant in olivine and have Cr#s 55–77 and Mg#s 12–36. Glass, pyroxene granules, microlitic plagioclase, ilmenite, and titanomagnetite comprise the groundmass.

**Lightning Creek.** The Lightning Creek basaltic andesite, also referred to as hybridized magmatic component or hybrid Lightning Creek unit, has 20–30% phenocrysts in a hypocrystalline groundmass (Table 1). Plagioclase (40–60% of phenocrysts) is euhedral to subhedral, up to 4.3 mm in length, and has three populations, (1) finely sieved cores with mid An (65–66 with $An_{48}$ outlier), (2) finely sieved rims with low An cores (42–44), and (3) coarsely sieved with variable An (47–89). Clinopyroxene (20–30%) is euhedral to anhedral and 0.3–1.5 mm in size. Clinopyroxene cores are divisible into a high Mg# (86–89) population with variable Cr (550–2700 ppm, positively correlated) and a mid Mg# (80–84) population with low Cr (100–460 ppm, no correlation). Both clinopyroxene populations exhibit normal and reverse zoning. Olivine (15–20%) is mostly euhedral, 0.25–3.5 mm in size, and has high core Fo (89–90) that is positively correlated with Ni (1800–3900 ppm; Figure 5). Rare, heavily embayed, $Fo_{80}$ olivine grains are also present. Cr-spinel inclusions in olivine have Cr# 48–65 and Mg# 35–55. Orthopyroxene (5–10%) is subhedral to anhedral, has Mg# 77–82 cores, and consists of small (≤ 1.0 mm) crystals, though some larger, elongate crystals are present. The groundmass contains titanomagnetite, glass, and plagioclase that varies from microlitic to tabular.

**Lightning Creek Inclusions.** Two types of volcanic inclusions, one mafic and one intermediate, are sparsely present in the Lightning Creek unit. Both inclusions are small (roughly 3 by 5 cm), and while disaggregated inclusion material is observed in all samples they are only present as individual, distinct inclusions in a single sample (Supplementary

Materials Figure 3). The mafic inclusion contains 5–7% phenocrysts of olivine and clinopyroxene (Table 1). Olivine (75–85% of phenocrysts) is euhedral to subhedral, 0.25–1.1 mm in diameter, and is compositionally similar (Fo 88–89; Figure 2) to the olivine found in the hybridized magmatic component. Clinopyroxene (15–25%) is subhedral, small (≤ 0.5 mm), and is compositionally comparable to the high Mg# clinopyroxene found in the hybridized magmatic component (Mg# 87; Figure 3). The groundmass is nearly holocrystalline and contains zoned microlitic plagioclase, clinopyroxene granules, acicular ilmenite, and some glass. The intermediate inclusion is porphyritic with 40–50% phenocrysts, which occur in clots (Table 1). Plagioclase (70–80% of phenocrysts) is euhedral to anhedral, variable in size (0.4–3.6 mm), and is $An_{47}$. Orthopyroxene (10–15%) is subhedral to anhedral, 0.5–2.0 mm in size, and has Mg# 65–70 cores. Clinopyroxene (5–10%) is subhedral to anhedral, 0.25–1.0 mm in size, has Mg# 75–80 cores, and exhibits reverse zoning. Both pyroxenes contain abundant oxide inclusions. Olivine (5%) is anhedral, up to 0.5 mm in size, and has Fo 78–82 cores. The groundmass is hypocrystalline with acicular to bladed ilmenite and titanomagnetite, tabular to microlitic plagioclase, and glass.

## Whole Rock Geochemical Data

Whole rock analyses were reported by Moore and DeBari (2012) and Mullen and McCallum (2014) for the Tarn Plateau HMBA, Baggerman and DeBari (2011) for the Glacier Creek HMA, and Taylor (2001) for the hybrid Lightning Creek HMBA. The rock units are subalkaline and calcalkaline per Irvine and Baragar (1971) and fall in the medium-K range of Gill (1981). New Lightning Creek analyses of a basaltic andesite mafic inclusion, an

andesitic intermediate inclusion, and a hybridized magmatic component are presented in Table 3. These three samples are also calcalkaline and fall in the medium-K range.

Select major elements are shown in Figure 6. Tarn Plateau HMBA has 51.8–54.0 wt% $SiO_2$ and Mg# 68–70, and the Glacier Creek HMA has 58.3–58.7 wt% $SiO_2$ and Mg# 63–64. Hybrid Lightning Creek HMBA has 54.8–56.4 $SiO_2$ and Mg# 70–73, the mafic inclusion has 54.6 wt% $SiO_2$ and Mg# 72, and the intermediate inclusion has 57.3 wt% $SiO_2$ and Mg# 61. Except for the most mafic Tarn Plateau sample, all three rock units display typical major element behavior observed in calcalkaline lavas, wherein $Na_2O$ increases and MgO and CaO decrease with $SiO_2$. Notable trace element contents and ratios include high Sr (≥ 770 ppm) and moderate Y (15–19 ppm) and Ba/Zr (2–4) in all three units, high Ni (≥ 67 ppm) in the Glacier Creek and Lightning Creek units, and high Cr (≥ 200 ppm) in the Tarn Plateau and Lightning Creek units. The Lightning Creek mafic inclusion is compositionally similar to hybrid Lightning Creek samples but has higher Sr (930 ppm) and Cr (290 ppm) contents. In contrast, the intermediate inclusion has higher Y (22 ppm) and lower Ni (64 ppm), Sr (600 ppm), and Cr (110 ppm) contents. Both inclusions have lower Ba/Zr (2) than hybrid Lightning Creek samples. Though hybrid Lightning Creek samples often plot between the mafic and intermediate inclusions, a clear mixing trend is not observed (Figures 6–7). However, evidence for mixing between primitive Lightning Creek HMBA samples and a crustally-derived dacitic endmember, and the production of the Lightning Creek HMA (57.3–58.0 wt% $SiO_2$, not shown here), are discussed in DeBari et al. (in review).

A primitive mantle-normalized diagram (Figure 8a) shows the characteristic enrichments in large ion lithophile elements (LILE: Cs, Rb, Ba, Th, U, K, and Sr) that are

typical of subduction-related magmatism. HREE depletions resulting in high Nd/Yb (≥ 10; Figure 7a) are observed in the North Cascades HMA and HMBA, but are less pronounced than depletions in Aleutian adakites (Nd/Yb ≥ 55; Figure 7a), which are also more enriched in LREE (Figure 8b). Mount Shasta primitive HMA (PMA; Grove et al. 2002) has lower HREE contents than the North Cascades units, but its Nd/Yb ratio (~12) and Sr contents (~800 ppm) are similar (Figure 7a). Compared to non-HMA calcalkaline basalts (CAB) and dacites from their respective volcanic field, the North Cascades units exhibit steeper REE patterns (Figure 8c–d). In the Mount Baker units this steepness is due to relative depletions in HREE compared to non-HMA units. In the Glacier Peak unit, the relative steepness is more a result of LREE enrichment compared to non-HMA rather than HREE depletion.

**Isotopic compositions.** Sr, Nd, and Pb isotopic compositions of the Tarn Plateau and Lightning Creek HMBA have been previously analyzed by DeBari et al. (in review), Moore and DeBari (2012), and Mullen and McCallum (2014), and a new Glacier Creek HMA analysis is presented in Table 4. Isotopic compositions of the three rock units are comparable to those of non-HMA primitive lavas from Mount Baker and Glacier Peak (Figure 9).

## Clinopyroxene Trace Element Data

Trace element (REE and Sr) concentrations in clinopyroxene are presented in Table 2. REE abundances in analyzed clinopyroxene correlate with their respective whole rock $SiO_2$ contents; the most $SiO_2$-poor rock unit, Tarn Plateau, has the lowest clinopyroxene REE abundances, and the most $SiO_2$-rich rock unit, Glacier Creek, has the highest clinopyroxene REE abundances (Figure 10). Clinopyroxene cores from both Mount Baker units show a

negative correlation between Mg# and Yb contents (Figure 11a), and cores from all three units show a positive correlation between Mg# and Sr contents (Figure 11c).

Measured clinopyroxene REE ratios were compared to calculated equilibrium clinopyroxene REE ratios (Nd/Yb) that were derived using clinopyroxene/liquid partition coefficients (Kds) and whole rock trace element data. We call the calculated ratios REE Equilibrium Clinopyroxene (REC). We present REC as Chondrite-normalized Nd/Yb, $(Nd/Yb)_{REC} = [(Nd_{Kd}/Yb_{Kd}) * \text{average } (Nd/Yb)_{N\ whole\ rock}]$. Kds were selected based on whole rock $SiO_2$ and $H_2O$ contents, mineral assemblages, pressure conditions, and number of Kds available. Kds were taken from Gaetani et al. (2003; hydrous spinel peridotite) for the Tarn Plateau and Lightning Creek HMBA and Fujimaki et al. (1984; semi-hydrous calcalkaline andesite) for the Glacier Creek HMA (Table 5). $(Nd/Yb)_N$ was also used to determine if steep clinopyroxene REE signatures are associated with high or low Mg# in the same clinopyroxene (Figures 11b and 12). In addition, we calculated REE Equilibrium Liquid (REL) compositions using the same Kds, and compared individual clinopyroxene REE patterns to whole rock REE patterns (Figure 13).

Tarn Plateau clinopyroxene exhibit a positive correlation between clinopyroxene Mg# and $(Nd/Yb)_N$ (Figures 11b and 12), and clinopyroxene REE patterns are more variable than expected for crystals equilibrated with a single parent melt. Distinct trends are identified when grains are separated into their Mg# groups (Figures 11 and 13a). REL of high Mg# clinopyroxene have steeper REE patterns than the whole rock, and differences between core and rim REL are generally minimal. High Mg# clinopyroxene also has the highest Sr contents (Figure 11c), indicating that the higher Nd/Yb and Mg# component is Sr-enriched.

REL of low Mg# clinopyroxene generally have similar REE trends as the host rock, and lower Sr contents.

Glacier Creek clinopyroxene has a narrow range of $(Nd/Yb)_N$ values, and does not exhibit a correlation between Mg# and $(Nd/Yb)_N$ (Figure 11b). In most cases, REL calculated from clinopyroxene cores and rims are higher and slightly steeper than the host rock, and show no variation despite pronounced Mg# increase in rims (Figure 13b). Though there is a slight increase in Sr with Mg# (up to Mg# 81; Figure 11c), the highest Mg# rims have comparable Sr contents relative to their lower Mg# cores, demonstrating no clear correlation between Mg# and Sr. This clinopyroxene has Eu depletion in both cores and rims, indicating co-crystallization with plagioclase throughout its crystallization history (Figures 10 and 13b).

Due to abundant mineral and glass inclusions in Lightning Creek clinopyroxene, core and rim analysis pairs were only successfully obtained for the high Mg# clinopyroxene in the hybridized magmatic component. Measured $(Nd/Yb)_N$ values of high Mg# clinopyroxene cores plot at higher $(Nd/Yb)_N$ than calculated REC of the hybrid Lightning Creek unit and mafic inclusion (Figure 11b). There is also no clear correlation between Mg# and $(Nd/Yb)_N$ in this clinopyroxene. Core and rim REL of this population show similar HREE abundances relative to the host rock, but are consistently more LREE-enriched (Figure 13c). As a result, REL of the high Mg# clinopyroxene population have steeper REE signatures compared to the whole rock. Sr contents in the high Mg# clinopyroxene show a moderately positive correlation with Mg# (Figure 11c). This indicates that Sr contents are correlated with Mg# and steeper Nd/Yb in the Lightning Creek hybridized magmatic component.

## DISCUSSION

## Crystallization Conditions

**Temperature and Pressure.** We use olivine and pyroxene thermobarometers to determine crystallization conditions of primitive components. Whole rock data were used for liquid compositions, and only phenocrysts in equilibrium with the whole rock were used for thermobarometry. Results, equilibrium Kds, and number of minerals used in calculations are listed in Table 6, and minimum values are listed below. A two-pyroxene thermobarometer (Putirka 2008) was used for the Glacier Creek (1,009 ± 56°C, 3.1 ± 2.8 kbar) and hybridized Lightning Creek units (999 ± 56°C, 1.6 ± 2.8 kbar). A clinopyroxene-liquid thermobarometer (Putirka 2008) was used for the Tarn Plateau unit because of the paucity of orthopyroxene. Tarn Plateau high Mg# clinopyroxene yielded a temperature of 1,087 ± 42°C and pressure of 8.3 ± 3.6 kbar, but low Mg# clinopyroxene is not in equilibrium with the whole rock and was therefore not used for thermobarometry (Figure 3b). Calculations are within range of previously reported conditions by Baggerman and DeBari (2011), Moore and DeBari (2012), and Mullen and McCallum (2014). The Lightning Creek mafic inclusion has no analyzed clinopyroxene, thus the olivine-liquid thermometer of Putirka (2008) was used, and yielded a temperature of 1,192 ± 43°C. The whole rock silica activity geobarometer of Putirka (2008) yielded an equilibrium pressure of 5.9 ± 2.9 kbar for the mafic inclusion. These results suggest similar equilibration temperatures for all units, except for the higher temperature of the Lightning Creek mafic inclusion. Depth differences between the units cannot be distinguished due to the high error associated with calculated equilibrium pressures.

**$H_2O$ Contents.** We use the Mitchell and Grove (2015) primitive andesites model to obtain $H_2O$ contents (Table 7). This model uses whole rock data and a fixed pressure to

calculate temperature and $H_2O$ contents with mean average errors of ± 23°C and ± 1.4 wt%, respectively. Only some samples from the Tarn Plateau and Lightning Creek HMBA had suitable compositional characteristics for this model (Mg# ≥ 70, $SiO_2$ ≥ 51 wt%, MgO ≥7 wt%, $K_2O$ ≤ 3 wt%, $TiO_2$ ≥ 0.4 wt%). Temperatures yielded by the model were consistently lower than those calculated using mafic minerals (Table 6). Tarn Plateau samples yielded minimum $H_2O$ contents of 5.8 wt%. Hybridized Lightning Creek samples yielded minimum $H_2O$ contents of 2.3 wt%, and the Lightning Creek mafic inclusion sample yielded 4.3 wt% $H_2O$. These $H_2O$ contents are within range of other Cascades and global primitive andesites presented in Mitchell and Grove (2015), but are higher than previous results for Tarn Plateau HMBA from Moore and DeBari (2012; 4.0 wt% $H_2O$) and Mullen and McCallum (2014; 3.4 wt% $H_2O$), and for Lightning Creek HMBA from Taylor (2001; 2.2 wt% $H_2O$). These earlier studies used plagioclase and whole rock compositions to calculate $H_2O$ contents (Sisson and Grove 1993; Lange et al. 2009). Calculations done for this study using the Lange et al. (2009) plagioclase hygrometer also yielded lower values for the Tarn Plateau and Lightning Creek HMBA (2.6–3.1 and 1.5–2.2 ± 0.32 wt% $H_2O$, respectively) and yielded 1.6–2.4 wt% ± 0.32 $H_2O$ for the Glacier Creek HMA, all of which are similar to Sisson and Grove (1993) model estimates (Table 7). However, since both of these methods yield $H_2O$ contents during plagioclase crystallization they may not reflect the $H_2O$ content of the primitive magmas.

Normalized whole rock Sr/P ratios of the HMA and HMBA were also examined because $(Sr/P)_N$ has been shown to correlate with $H_2O$ contents (Figure 14; Borg et al. 1997). Since Sr is fluid-mobile and P is fluid-immobile, high $(Sr/P)_N$ contents (≥ 3.3; Clynne and Borg 1997) indicate a hydrous source. $(Sr/P)_N$ values in all three rock units are higher than

those of non-HMA from their respective volcanic fields (> 3.3 in the Mount Baker units and the Lightning Creek mafic inclusion compared to < 2.5 in the non-HMA units).

**Role for Garnet Fractionation**

Most hypotheses for HMA origin include an important role for the involvement of residual garnet as the driver for steep REE patterns (Stern and Kilian 1996; Yogodzinski and Kelemen 1998, 2007; Kelemen et al. 2003; Martin et al. 2005; Macpherson et al. 2006). There is no textural evidence (i.e. remnant garnet phenocrysts) for the presence of fractionating garnet in the HMA and HMBA studied here, nor is there preserved mineral geochemical evidence as even the most primitive clinopyroxene indicates crystallization from a parental magma that already had a steep REE pattern. Specifically, there is no progressive change from flat to steep REE patterns in clinopyroxene phenocrysts that would indicate garnet co-crystallization. If garnet crystallized early, that mineral, and any other co-crystallizing phases, would have to have been completely removed via fractionation. Nonetheless, the feasibility of this hypothesis was examined using simple mass-balance fractionation modeling. The modeling tests whether the HMA and HMBA can be produced from a typical Cascades CAB through high pressure fractional crystallization of a pyroxene, garnet, and amphibole assemblage, as hypothesized by Macpherson et al. (2006). This mineral assemblage (±olivine) is predicted in a hydrous, high pressure arc setting (> 3 wt% $H_2O$ and 1.2 GPa; Müntener et al. 2001) such as that in the northern Cascade Arc, where the arc crust is ~35 km thick (Syracuse et al. 2010). North Cascades CAB from Mount Baker and Glacier Peak were selected as parents for modeling based on their primitive compositions.

Modeling results show that major element compositions of the HMA and HMBA are not reproducible via fractionation of a pyroxene, olivine, and garnet ±amphibole assemblage using regional primitive CAB compositions as parents (Figure 15e–f). Though HMA and HMBA Sr/Y, Y, and LREE contents can be reproduced using the Mount Baker CAB (Lake Shannon, 50.7 wt% $SiO_2$, Mg# 62; Moore and DeBari 2012), high garnet contents (≥ 38%) and a high percentage of fractionation (~60%) are required, and even higher percentages of fractionation (≥ 80%) are needed to reproduce similar HREE contents (Figure 15a and c). These high fractionation percentages are not realistic given the high Mg# of clinopyroxene phenocrysts. We thus discount using garnet fractionation in any model for the formation of the three North Cascades units studied here. This is in agreement with Mullen and McCallum (2014), who determined that Dy/Yb values are too low to be indicative of garnet fractionation in Mount Baker primitive magmas.

**Isotopic Constraints on Mantle and Crustal Contributions**

Tarn Plateau and Lightning Creek HMBA compositions are among the more isotopically depleted Cascade calcalkaline magmas, and though the Glacier Creek HMA is more enriched than the two HMBA, it is on par with other Mount Baker primitive lavas (Figure 9). The three rock units are not as isotopically depleted as most Juan de Fuca mid-ocean ridge basalt (MORB) isotopic compositions (White et al. 1987; Cousens et al. 1995), and are not as isotopically enriched as Cascadia sediment (Plank and Langmuir 1998). They do, however, fall on a possible mixing trend between Juan de Fuca MORB and Cascadia sediment compositions, as noted by Mullen and McCallum (2014). Some samples from the hybrid Lightning Creek unit show isotopic enrichment (Figure 9), but that enrichment

directly correlates with $SiO_2$ contents that DeBari et al. (in review) interpret to be evidence for progressive mixing with the more isotopically enriched Glacier Peak dacite. The most isotopically depleted Lightning Creek sample is the most primitive, and is representative of the mantle component.

For the three rock units, isotopic compositions of the most primitive samples denote a mantle origin with no substantial involvement of the overriding crust. This result has important petrogenetic implications for the primitive arc andesites and basaltic andesites in this study. Specifically, the mineral assemblages in the primitive samples indicate contributions from multiple magmas, and the primitive nature of their isotopic character suggests that multiple mantle-generated melts and their derivatives are the source for this diversity rather than the crust (see petrogenesis section below and Figure 16). However, the more differentiated the sample, the more influential the crustal component may be, as is reflected in their more isotopically enriched characteristics (Figure 9).

## Petrogenesis of North Cascades High-Mg Andesites

**Tarn Plateau.** Two clinopyroxene populations, two plagioclase populations, one olivine population, and one orthopyroxene population in the Tarn Plateau HMBA imply that two magmas contributed crystals ± liquids to create a semi-homogenized hybrid (Table 1; Figures 2–4). The steepest $(Nd/Yb)_N$ ratios and highest Sr contents are observed in the highest Mg# clinopyroxene (Figure 12), and sector zoning in this clinopyroxene implies high pressure crystallization conditions (e.g. 5–10 kbar; Skulski et al. 1994), which are confirmed by the calculated pressure estimates (8.3 ± 3.6 kbar; Table 6). Therefore the REE steepness in this clinopyroxene population is a characteristic of a primitive, Sr-enriched, mantle-derived

mafic liquid. In addition to this primitive mantle-derived liquid, we propose the existence of a second, differentiated magma type (i.e., fractionated melt of mantle-derived basalt). This is based on the additional clinopyroxene population with lower Mg#, $(Nd/Yb)_N$, and Sr, and Eu depletions that signify co-crystallization with plagioclase. The hypothesis for this second, differentiated magma type is also supported by low olivine Fo values (which are too Fe-rich to be in equilibrium with peridotite), low olivine Ni contents, and the scarcity of Cr-spinel, all of which are suggestive of olivine fractionation. The overall low $Na_2O$, $K_2O$, $TiO_2$, and $Al_2O_3$ of the whole rock suggests a depleted mantle source for both magma types. Low olivine Ni contents also refute the Straub et al. (2008) pyroxenite melting model plausibility for this unit (see Glacier Creek discussion below and Figure 5).

Clinopyroxene populations from the Tarn Plateau unit exhibit similar geochemical characteristics to those reported in clinopyroxene of Aleutian adakites (Figure 11; Yogodzinski and Kelemen 1998). High Mg# clinopyroxene has the highest Sr and Nd/Yb core concentrations, which generally decrease, along with Mg#, in the rim. Low Mg# clinopyroxene has the lowest Sr and Nd/Yb core concentrations, which increase with Mg# in the rim. Yogodzinski and Kelemen (1998) describe these relationships as being due to mixing between (1) andesitic or dacitic melts derived from a garnet-bearing subducting slab, which became Mg-rich as they rose through and interacted with the overlying mantle wedge, and (2) basaltic melt derived from the asthenospheric mantle. Based on these Mg#, Nd/Yb, and Sr relationships in high Mg# clinopyroxene, the simultaneous increase in whole rock Mg# and $SiO_2$ contents (Figure 6a), high $H_2O$ contents (2.6–6.0 wt%, Table 7; Moore and DeBari 2012; Mullen and McCallum 2014), and high whole rock $(Sr/P)_N$ (Figure 14), we

interpret the primitive, Sr-enriched, mantle-derived mafic component of Tarn Plateau to be a hydrous slab melt that interacted with the overlying mantle. The slab melt component mixed with the differentiated mafic component near the Moho to produce the Tarn Plateau HMBA (Figure 16). Slab melt and fluid involvement in the generation of the Tarn Plateau HMBA is supported by Mullen and McCallum (2014), who used whole rock geochemistry, isotopic data, and modeling to conclude that a hydrated, down-dragged mantle peridotite interacts with slab and sediment melt to produce primitive magmas beneath Mount Baker.

**Glacier Creek.** The Glacier Creek HMA has a limited whole-rock composition (Figures 6-8), with at least two sources of input to the crystal cargo. Evidence for this comes from the two plagioclase populations, one clinopyroxene population, one orthopyroxene population, and one olivine population (Table 1; Figures 2–4). We interpret the olivine to be a single xenocrystic population because of monomineralic crystal clots, pronounced orthopyroxene reaction rims, lack of equilibrium with the host rock, and consistent Fo and Ni contents. The olivine addition hypothesis was first suggested for Glacier Creek by Baggerman and DeBari (2011), where the authors used petrographic observations and Fe/Mg equilibrium to calculate ~4% addition of xenocrystic olivine.

We thus interpret the Glacier Creek HMA to be comprised of a host magma that mixed with an olivine-bearing mafic component. Based on the abundance of plagioclase phenocrysts, low-Mg# pyroxenes, and extensive reaction rims observed on xenocrystic olivine, the host magma is interpreted to be intermediate (i.e. andesitic) in composition. Addition of the mafic component and concomitant resorption of the xenocrystic olivine would raise MgO contents in the host magma, leading to the observed Mg# increase in

clinopyroxene rims. Because Glacier Creek clinopyroxene REL and $(Nd/Yb)_N$ do not change from core to rim despite this significant change in Mg# (Figure 11), the steep REE pattern of the Glacier Creek host magma must have been acquired prior to clinopyroxene crystallization and incorporation of the mafic component. Consequently, the high Mg# and steep REE characteristics were obtained from different sources. The mafic component may have been added through incorporation of an olivine cumulate or an olivine-bearing magma with Nd/Yb similar to that of the Glacier Creek host magma. In either scenario, a high Mg# mafic component is added to a more silicic host magma with pre-existing elevated Nd/Yb.

Since the high Mg# and Nd/Yb characteristics of the Glacier Creek HMA were acquired from different components that mixed within the crust (3.1 ± 2.8 kbar; Table 6), we reject the slab melt hypothesis for this unit. The steep REE pattern cannot be a product of crustal melt incorporation as proposed by some workers (Stern and Kilian 1996; Richards and Kerrich 2007; Streck et al. 2007) because isotopic compositions do not support significant crustal involvement (Figure 9). Furthermore, HREE abundances in this rock unit are lower than HREE abundances in crustally-derived dacitic lavas from Mount Baker (Figure 8; Gross 2012), suggesting that the REE signature is not a result of mixing with crustal melts. Therefore we interpret the Glacier Creek HMA to be a differentiated mantle-derived melt with a long trajectory through the crust, but with minimal crustal incorporation. Additional evidence for this interpretation include the high abundance and diverse populations of plagioclase phenocrysts that indicate fractionation, and mid-crust pyroxene crystallization pressures (Table 6). This HMA does have significantly higher Sr contents and $(Sr/P)_N$ compared to other non-HMA lavas from Mount Baker (Figure 14), as well as

moderate $H_2O$ contents (1.6–2.4 wt% $H_2O$, Table 7), suggesting that the mantle source for the Glacier Creek unit was ultimately fluxed by a hydrous slab component that was enriched in incompatible elements and had moderate Nd/Yb (Borg et al. 1997; Clynne and Borg 1997; Grove et al. 2002, 2005). This moderate Nd/Yb mantle melt underwent differentiation within the crust, incorporated the xenocrystic high-Ni olivine and potentially minor crustal components, and was erupted as a hybrid HMA (Figure 16).

The cause for high Ni relative to Fo in the xenocrystic (Figure 5) olivine is debatable, and its source prior to incorporation in the Glacier Creek HMA remains unconstrained. Straub et al. (2008, 2011) contend that high Ni contents in phenocrystic olivine originate from melts of secondary mantle pyroxenite lithologies that formed by infiltration of silicic slab components. This reaction pyroxenite is Ni-rich, but has less capacity to retain Ni in the source than peridotite, consequently producing Ni-rich melts capable of crystallizing high-Ni olivine. Alternatively, high-Ni olivine may crystallize from a mixture of high-MgO mantle partial melts and low-MgO crustal or eclogite partial melts (e.g. Wang and Gaetani 2008) that yields hybrid melts with an increased Ni compatibility in olivine (Hart and Davis 1978).

**Lightning Creek.** The Lightning Creek HMBA is a hybrid magma with four plagioclase populations, three clinopyroxene populations, two olivine populations, and two orthopyroxene populations (including mafic and intermediate inclusions mineral populations; Table 1; Figures 2–4). A major component of the Lightning Creek magma is the liquid represented by the mafic inclusion, which is a viable mafic mixing endmember to the hybrid Lightning Creek unit (Figures 6–8). Therefore the hybrid Lightning Creek high Mg# clinopyroxene and high Fo olivine populations are interpreted to be derived directly from the

mafic inclusion magma over time. A second component is Glacier Peak dacite, which DeBari et al. (in review) show to be the silicic mixing endmember of the hybrid Lightning Creek unit. DeBari et al. (in review) used isotopic data and major and trace element mixing models to reproduce whole rock trends observed in the hybrid Lightning Creek unit, and concluded that this felsic Glacier Peak endmember is crustal in origin and is not the source for the steep REE, which agrees with data from this study. The intermediate inclusion represents a compositionally distinct magmatic component with low Nd/Yb and $(Sr/P)_N$ (Figure 14). Only the low Fo olivine, low Mg# pyroxenes, and $An_{47}$ plagioclase populations are found in the intermediate inclusion and are interpreted to be cognate to the inclusion. Compositionally, this inclusion does not appear to be a major contributor to this unit.

The mafic Lightning Creek inclusion is the magmatic component with the steepest REE pattern and highest MgO and Sr contents. Fo and Ni contents of high Fo olivine are not high enough to fit the Straub et al. (2008, 2011) HMA hypothesis for melts of a pyroxenitized mantle source (Figure 5). Instead, a combination of high Cr-spinel Cr# and high host olivine Fo contents suggest magma derivation from a depleted, olivine-rich mantle source (Supplementary Materials Figure 5). Arai (1987) shows that Cr# in mantle Cr-spinel increases as the mantle becomes more depleted, and that Cr# in Cr-spinel and Fo contents in olivine are positively correlated. We observe this correlation of high Cr# and Fo contents in the mafic Lightning Creek inclusion, as did Clynne and Borg (1997) in southern Cascade Arc CAB. High whole rock $H_2O$ (4.3 wt%) and Sr contents, and elevated whole rock and clinopyroxene $(Nd/Yb)_N$, indicate that the refractory mantle source of the mafic inclusion was hydrated by a LILE-enriched slab component (Borg et al. 1997; Clynne and Borg 1997;

Grove et al. 2002). Hydrous melting of a depleted mantle likely resulted in the elevated $SiO_2$ (~55 wt%) contents of the mafic inclusion (Grove et al. 2002, 2005). Consequently, the hybrid Lightning Creek unit acquired its HMBA characteristics, high Mg#, steep REE, high Ni and Cr, and elevated $SiO_2$, from the mafic inclusion through its mantle source and associated hydrous slab component (Figure 16). Lack of isotopic enrichment in primitive Lightning Creek samples containing crystal cargo from the intermediate inclusion (Figure 9) suggests that the intermediate inclusion must itself be a fractionated mantle-derived component, not a crustally-derived component. The mafic inclusion magma mixed with the intermediate inclusion and Glacier Peak dacite magmas in the crust to produce the hybrid Lightning Creek unit.

## CONCLUSIONS

Petrography and mineral geochemistry of multiple phenocryst populations, interpreted in conjunction with whole rock chemistry, demonstrate that three high-Mg lavas from the Mount Baker Volcanic Field and Glacier Peak in the northern Cascade Arc have complex origins involving mixing of a variety of magmatic components. A single process cannot explain the Mg# and REE characteristics of the HMA and HMBA studied here, and multiple mantle sources are indicated. Furthermore, in no case is the crust interpreted to be the source for the steep REE patterns of these rock units.

The high Mg# and Nd/Yb characteristics of all three rock units were diluted and partially obscured by interaction with non-HMA components. The Tarn Plateau HMBA from Mount Baker has an origin similar to Aleutian adakites and is a hybrid of two magmatic components, one of which is a clinopyroxene-bearing HMA component that shows evidence

for being a high Nd/Yb slab melt, presumably with elevated $SiO_2$ contents, that interacted with the mantle. This component underwent mixing near the base of the crust with a mantle-derived basaltic component to produce the Tarn Plateau HMBA. Mount Baker's Glacier Creek unit has two identifiable components, an andesitic host melt with elevated Nd/Yb and Sr and an olivine-bearing mafic component. The andesitic host melt differentiated from partial melts of the mantle and equilibrated at shallow levels where it incorporated the mafic component, which increased whole rock MgO and Ni contents and resulted in reversely zoned clinopyroxene rims. The characteristic steep whole rock REE pattern is a melt characteristic that resulted from mantle melting through hydration by a LILE-enriched slab component. Glacier Peak's Lightning Creek HMBA is a hybrid product that has at least three magmatic components, only one of which exhibits HMA characteristics and is interpreted to have originated from depleted mantle by fluxing with a LILE-enriched, hydrous slab component. Differentiation or a high degree of melting resulted in the elevated $SiO_2$ contents. Subsequently, the HMA component mixed with more evolved (but lower La/Yb) melts in Glacier Peak's shallow magmatic system in the middle-to-upper crust.

The complexity of mineral populations indicate that there were small pockets of magma in the plumbing systems of Mount Baker and Glacier Peak. The preservation of these different mineral populations, including minerals that represent HMA components with high Mg# and elevated Nd/Yb, suggests that at the time these units erupted there was no large standing magma body capable of absorbing and obscuring individual mineral compositions beneath the volcanoes, or that mixing occurred shortly before eruption. This is especially pertinent for the Tarn Plateau and Lightning Creek HMBA, whose HMA components were

identifiable despite being complex hybridized products. This is not always typical for large composite volcanoes, which often erupt the small or very similar homogeneous lithologies for long periods of their history. Furthermore, most components that contributed to phenocryst diversity originated in the mantle, indicating that mantle, not crustal, processes are dominantly responsible for the heterogeneity of these arc lavas.

## IMPLICATIONS

Work over the last few decades has increasingly shown that magmas erupted from composite volcanoes in volcanic arcs are typically products of open system processes at all stages of their origin, and that crustal processes are not necessarily the main drivers for compositional diversity observed in arc magmas. Moreover, generalized whole rock studies and simple fractionation modeling are often inadequate to explain magma origin and evolution. We emphasize the necessity of careful petrography and the power of mineral chemical analyses to identify populations of phenocrysts and relate them to often cryptic components in arc magmas identified by geochemical techniques. In particular, analysis of clinopyroxene REE compositions is useful for recognizing contributions from the subducting slab, such as the Tarn Plateau slab melt component identified in this study. Employment of this type of study in the future will continue to improve our understanding of the complexity of arc magma generation and evolution processes.

## ACKNOWLEDGMENTS

This study was possible thanks to financial support to M. Sas from the Evolving Earth Foundation, Geological Society of America, Mount Baker Volcano Research Center, and

Western Washington University. We acknowledge the Western Washington University AMSEC for access to the LA-ICP-MS and Sci-Tech for access to the SEM. We also thank S. Straub, M. Stelten, G. Yogodzinski, and E. Mullen for their reviews and improvement of this manuscript. Any use of trade, firm, or product names is for descriptive purposes only and does not imply endorsement by the U.S. Government.

## REFERENCES

Arai, S. (1987) An estimation of the least depleted spinel peridotite on the basis of olivine-spinel mantle array. Neues Jahrbuch fur Mineralogie-Monatshefte, 1987, 347–354.

Armstrong, J.T. (1988a) Bence-Albee after 20 years: review of the accuracy of α-factor correction procedures for oxide and silicate minerals. In D.E. Newbury, Ed., Microbeam Analysis, p. 469–476. San Francisco Press.

——— (1988b) Quantitative analysis of silicate and oxide minerals: comparison of Monte Carlo, ZAF and phi-rho-z procedures In D E. Newbury, Ed., Microbeam Analysis, p. 239–246. San Francisco Press.

Bacon, C.R., Gunn, S.H., Lanphere, M.A., and Wooden, J.L. (1994) Multiple isotopic components in Quaternary volcanic rocks of the Cascade Arc near Crater lake, Oregon. Journal of Petrology, 35, 1521–1556.

Bacon, C.R., Bruggman, P.E., Christiansen, R.L., Clynne, M.A., Donnelly-Nolan, J.M., and Hildreth, W. (1997) Primitive magmas at five Cascades volcanic fields: melts from hot, heterogeneous sub-arc mantle. Canadian Mineralogist, 35, 397–424.

Baggerman, T.D., and DeBari, S.M. (2011) The generation of a diverse suite of Late Pleistocene and Holocene basalt through dacite lavas from the northern Cascade arc at Mount Baker, Washington. Contributions to Mineralogy and Petrology, 161, 75–99.

Baker, M.B., Grove, T.L., Kinzler, R.J., Donnelly-Nolan, J.M., and Wandless, G.A. (1991) Origin of compositional zonation (high-alumina basalt to basaltic andesite) in the Giant Crater Lava Field, Medicine Lake volcano, Northern California. Journal of Geophysical Research, 96, 21819–21842.

Borg, L.E., and Clynne, M.A. (1998) The petrogenesis of felsic calc-alkaline magmas from the southernmost Cascades, California: origin by partial melting of basaltic lower crust. Journal of Petrology, 39, 1197–1222.

Borg, L.E., Clynne, M.A., and Bullen, T.D. (1997) The variable role of slab-derived fluids in the generation of a suite of primitive calc-alkaline lavas from the southernmost Cascades, California. Canadian Mineralogist, 35, 425–452.

Borg, L.E., Blichert-Toft, J., and Clynne, M.A. (2002) Ancient and modern subduction zone contributions to the mantle sources of lavas from the Lassen region of California inferred from Lu–Hf isotopic systematics. Journal of Petrology, 43, 705–723.

Brach-Papa, C., Van Bocxstaele, M., Ponzevera, E., and Quétel, C.R. (2009) Fit for purpose validated method for the determination of the strontium isotopic signature in mineral water samples by multi-collector inductively coupled plasma mass spectrometry. Spectrochimica Acta Part B: Atomic Spectroscopy, 64, 229–234.

Braunmiller, J., and Nábělek, J. (2002) Seismotectonics of the Explorer region. Journal of Geophysical Research, 107, 2208.

Bullen, T.D., and Clynne, M.A. (1990) Trace element and isotopic constraints on magmatic evolution at Lassen Volcanic Center. Journal of Geophysical Research, 95, 19671-19691.

Calmus, T., Aguillón-Robles, A., Maury, R.C., Bellon, H., Benoit, M., Cotten, J., Bourgois, J., and Michaud, F. (2003) Spatial and temporal evolution of basalts and magnesian andesites ("bajaites") from Baja California, Mexico: the role of slab melts. Lithos, 66, 77–105.

Chiaradia, M., Merino, D., and Spikings, R. (2009) Rapid transition to long-lived deep crustal magmatic maturation and the formation of giant porphyry-related mineralization (Yanacocha, Peru). Earth and Planetary Science Letters, 288, 505–515.

Church, S.E. (1976) The Cascade Mountains revisited: A re-evaluation in light of new lead isotopic data. Earth and Planetary Science Letters, 29, 175–188.

Clynne, M.A. (1993) Geologic studies of the Lassen Volcanic Center, Cascade Range, California, 404 p. Ph.D. dissertation, University of California Santa Cruz.

Clynne, M.A., and Borg, L.E. (1997) Olivine and chromian spinel in primitive calc-alkaline and tholeiitic lavas from the southernmost Cascade Range, California: a reflection of relative fertility of the source. Canadian Mineralogist, 35, 453–472.

Conrey, R.M., Hooper, P.R., Larson, P.B., Chesley, J., and Ruiz, J. (2001) Trace element and isotopic evidence for two types of crustal melting beneath a High Cascade volcanic center, Mt. Jefferson, Oregon. Contributions to Mineralogy and Petrology, 141, 710–732.

Cooper, L.B., Plank, T., Arculus, R.J., Hauri, E.H., Hall, P.S., and Parman, S.W. (2010) High-Ca boninites from the active Tonga Arc. Journal of Geophysical Research, 115, B10206.

Cousens, B.L., Allan, J.F., Leybourne, M.I., Chase, R.L., and Van Wagoner, N. (1995) Mixing of magmas from enriched and depleted mantle sources in the northeast Pacific: West Valley segment, Juan de Fuca Ridge. Contributions to Mineralogy and Petrology, 120, 337–357.

Crawford, A.J., Falloon, T.J., and Green, D.H. (1989) Classification, petrogenesis and tectonic setting of boninites. In A.J. Crawford, Ed., Boninites, p. 1–49. Unwin Hyman, London.

Defant, M.J., and Drummond, M.S. (1990) Derivation of some modern arc magmas by melting of young subducted lithosphere. Nature, 347, 662–665.

Falloon, T.J., Danyushevsky, L.V., Crawford, A.J., Meffre, S., Woodhead, J.D., and Bloomer, S.H. (2008) Boninites and Adakites from the Northern Termination of the Tonga Trench: Implications for Adakite Petrogenesis. Journal of Petrology, 49, 697–715.

Fujimaki, H., Tatsumoto, M., and Aoki, K. (1984) Partition coefficients of Hf, Zr, and REE between phenocrysts and groundmasses. Journal of Geophysical Research, 89, B662–B672.

Gaetani, G.A., Kent, A.J.R., Grove, T.L., Hutcheon, I.D., and Stolper, E.M. (2003) Mineral/melt partitioning of trace elements during hydrous peridotite partial melting. Contributions to Mineralogy and Petrology, 145, 391–405.

Gaffney, A.M., Blichert-Toft, J., Nelson, B.K., Bizzarro, M., Rosing, M., and Albarède, F. (2007) Constraints on source-forming processes of West Greenland kimberlites inferred from Hf–Nd isotope systematics. Geochimica et Cosmochimica Acta, 71, 2820–2836.

Gill, J.B. (1981) Orogenic andesites and plate tectonics, 390 p. Springer-Verlag, Berlin.

Green, N.L. (2006) Influence of slab thermal structure on basalt source regions and melting conditions: REE and HFSE constraints from the Garibaldi volcanic belt, northern Cascadia subduction system. Lithos, 87, 23–49.

Green, N.L., and Harry, D.L. (1999) On the relationship between subducted slab age and arc basalt petrogenesis, Cascadia subduction system, North America. Earth and planetary science letters, 171, 367–381.

Green, N.L., and Sinha, A.K. (2005) Consequences of varied slab age and thermal structure on enrichment processes in the sub-arc mantle of the northern Cascadia subduction system. Journal of Volcanology and Geothermal Research, 140, 107–132.

Gross, J.A. (2012) Felsic magmas from Mt. Baker in the northern Cascade arc: origin and role in andesite production, 111 p. M.S. thesis, Western Washington University, Bellingham.

Grove, T., Parman, S., Bowring, S., Price, R., and Baker, M. (2002) The role of an $H_2O$-rich fluid component in the generation of primitive basaltic andesites and andesites from the Mt. Shasta region, N California. Contributions to Mineralogy and Petrology, 142, 375–396.

Grove, T.L., Kinzler, R.J., Baker, M.B., Donnelly-Nolan, J.M., and Lesher, C.E. (1988) Assimilation of granite by basaltic magma at Burnt Lava flow, Medicine Lake volcano, northern California: decoupling of heat and mass transfer. Contributions to Mineralogy and Petrology, 99, 320–343.

Grove, T.L., Baker, M.B., Price, R.C., Parman, S.W., Elkins-Tanton, L.T., Chatterjee, N., and Müntener, O. (2005) Magnesian andesite and dacite lavas from Mt. Shasta, northern California: products of fractional crystallization of $H_2O$-rich mantle melts. Contributions to Mineralogy and Petrology, 148, 542–565.

Guffanti, M., and Weaver, C.S. (1988) Distribution of late Cenozoic volcanic vents in the Cascade Range: Volcanic arc segmentation and regional tectonic considerations. Journal of Geophysical Research, 93, 6513–6529.

Guillong, M., Meier, D.L., Allan, M.M., Heinrich, C.A., and Yardley, B.W.D. (2008) SILLS: A MATLAB-based program for the reduction of laser ablation ICP–MS data of homogeneous materials and inclusions. In P.J. Sylvester, Ed., Laser Ablation-ICP-MS

in the Earth Sciences: Current practices and outstanding issues, 40, p. 328–333. Mineralogical Association of Canada, Vancouver.

Harkins, S.A., Appold, M.S., Nelson, B.K., Brewer, A.M., and Groves, I.M. (2008) Lead isotope constraints on the origin of nonsulfide zinc and sulfide zinc-lead deposits in the Flinders Ranges, South Australia. Economic Geology, 103, 353–364.

Hart, S.R. (1984) A large-scale isotope anomaly in the Southern Hemisphere mantle. Nature, 309, 753–757.

Hart, S.R., and Davis, K.E. (1978) Nickel partitioning between olivine and silicate melt. Earth and Planetary Science Letters, 40, 203–219.

Hildreth, W., Fierstein, J., and Lanphere, M. (2003) Eruptive history and geochronology of the Mount Baker volcanic field, Washington. Geological Society of America Bulletin, 115, 729–764.

Irvine, Tn., and Baragar, Wra. (1971) A guide to the chemical classification of the common volcanic rocks. Canadian Journal of Earth Sciences, 8, 523–548.

Jicha, B.R., Hart, G.L., Johnson, C.M., Hildreth, W., Beard, B.L., Shirey, S.B., and Valley, J.W. (2009) Isotopic and trace element constraints on the petrogenesis of lavas from the Mount Adams volcanic field, Washington. Contributions to Mineralogy and Petrology, 157, 189–207.

Jochum, K.P., Weis, U., Stoll, B., Kuzmin, D., Yang, Q., Raczek, I., Jacob, D.E., Stracke, A., Birbaum, K., Frick, D.A., and others (2011) Determination of reference values for

NIST SRM 610–617 glasses following ISO guidelines. Geostandards and Geoanalytical Research, 35, 397–429.

Johnson, D.M., Hooper, P.R., and Conrey, R.M. (1999) XRF analysis of rocks and minerals for major and trace elements on a single low dilution Li-tetraborate fused bead. Advances in X-ray Analysis, 41, 843–867.

Kay, R.W. (1978) Aleutian magnesian andesites: melts from subducted Pacific Ocean crust. Journal of Volcanology and Geothermal Research, 4, 117–132.

Kelemen, P.B., Yogodzinski, G.M., and Scholl, D.W. (2003) Along-strike variation in the Aleutian island arc: Genesis of high Mg# andesite and implications for continental crust. Geophysical Monograph Series, 138, 223–276.

Kim, J., and Jacobi, R.D. (2002) Boninites: characteristics and tectonic constraints, northeastern Appalachians. Physics and Chemistry of the Earth, 27, 109–147.

Knaack, C., Cornelius, S.B., and Hooper, P.R. (1994) Trace Element Analyses of Rocks and Minerals by ICP-MS. GeoAnalytical Lab, Washington State University.

Kushiro, I. (1969) The system forsterite-diopside-silica with and without water at high pressures. American Journal of Science, 267, 269–294.

Lange, R.A., Frey, H.M., and Hector, J. (2009) A thermodynamic model for the plagioclase-liquid hygrometer/thermometer. American Mineralogist, 94, 494–506.

Leeman, W.P., Smith, D.R., Hildreth, W., Palacz, Z., and Rogers, N. (1990) Compositional diversity of late Cenozoic basalts in a transect across the southern Washington Cascades: implications for subduction zone magmatism. Journal of Geophysical Research, 95, 19561–19582.

Leeman, W.P., Tonarini, S., Chan, L.H., and Borg, L.E. (2004) Boron and lithium isotopic variations in a hot subduction zone—the southern Washington Cascades. Chemical Geology, 212, 101–124.

Leeman, W.P., Lewis, J.F., Evarts, R.C., Conrey, R.M., and Streck, M.J. (2005) Petrologic constraints on the thermal structure of the Cascades arc. Journal of Volcanology and Geothermal Research, 140, 67–105.

Longerich, H.P., Jackson, S.E., and Günther, D. (1996) Laser ablation inductively coupled plasma mass spectrometric transient signal data acquisition and analyte concentration calculation. Journal of Analytical Atomic Spectrometry, 11, 899–904.

Macpherson, C.G., Dreher, S.T., and Thirlwall, M.F. (2006) Adakites without slab melting: High pressure differentiation of island arc magma, Mindanao, the Philippines. Earth and Planetary Science Letters, 243, 581–593.

Martin, H., Smithies, R.H., Rapp, R., Moyen, J.-F., and Champion, D. (2005) An overview of adakite, tonalite–trondhjemite–granodiorite (TTG), and sanukitoid: relationships and some implications for crustal evolution. Lithos, 79, 1–24.

Magna, T., Wiechert, U., Grove, T.L., and Halliday, A.N. (2006) Lithium isotope fractionation in the southern Cascadia subduction zone. Earth and Planetary Science Letters, 250, 428–443.

McCrory, P.A., Blair, J.L., Oppenheimer, D.H., and Walter, S.R. (2006) Depth to the Juan de Fuca slab beneath the Cascadia subduction margin: A 3-D model for sorting earthquakes. U.S. Geological Survey Data Series 91, p. 13. http://pubs.usgs.gov/ds/91/

McCrory, P.A., Blair, J.L., Waldhauser, F., and Oppenheimer, D.H. (2012) Juan de Fuca slab geometry and its relation to Wadati-Benioff zone seismicity. Journal of Geophysical Research, 117, B09306.

Mitchell, A.L., and Grove, T.L. (2015) Melting the hydrous, subarc mantle: the origin of primitive andesites. Contributions to Mineralogy and Petrology, 170, 13.

Mitchell, E.C., and Asmerom, Y. (2011) U-series isotope systematics of mafic magmas from central Oregon: Implications for fluid involvement and melting processes in the Cascade arc. Earth and Planetary Science Letters, 312, 378–389.

Moore, N.E., and DeBari, S.M. (2012) Mafic magmas from Mount Baker in the northern Cascade arc, Washington: probes into mantle and crustal processes. Contributions to Mineralogy and Petrology, 163, 521–546.

Mullen, E.K., and McCallum, I.S. (2014) Origin of Basalts in a Hot Subduction Setting: Petrological and Geochemical Insights from Mt. Baker, Northern Cascade Arc. Journal of Petrology, 55, 241–281.

Mullen, E.K., and Weis, D. (2013) Sr-Nd-Hf-Pb isotope and trace element evidence for the origin of alkalic basalts in the Garibaldi Belt, northern Cascade arc: Alkalic Basalts, Northern Cascade Arc. Geochemistry, Geophysics, Geosystems, 14, 3126–3155.

——— (2015) Evidence for trench-parallel mantle flow in the northern Cascade Arc from basalt geochemistry. Earth and Planetary Science Letters, 414, 100–107.

Müntener, O., Kelemen, P.B., and Grove, T.L. (2001) The role of $H_2O$ during crystallization of primitive arc magmas under uppermost mantle conditions and genesis of igneous pyroxenites: an experimental study. Contributions to Mineralogy and Petrology, 141, 643–658.

Nelson, B.K. (1995) Fluid flow in subduction zones: evidence from Nd-and Sr-isotope variations in metabasalts of the Franciscan complex, California. Contributions to Mineralogy and Petrology, 119, 247–262.

Oleskevich, D.A., Hyndman, R.D., and Wang, K. (1999) The updip and downdip limits to great subduction earthquakes: Thermal and structural models of Cascadia, south Alaska, SW Japan, and Chile. Journal of Geophysical Research, 104, 14965–14991.

Plank, T., and Langmuir, C.H. (1998) The chemical composition of subducting sediment and its consequences for the crust and mantle. Chemical Geology, 145, 325–394.

Putirka, K.D. (2008) Thermometers and barometers for volcanic systems. Reviews in Mineralogy and Geochemistry, 69, 61–120.

Richards, J.P., and Kerrich, R. (2007) Adakite-like rocks: their diverse origins and questionable role in metallogenesis. Economic Geology, 102, 537–576.

Ruscitto, D.M., Wallace, P.J., and Kent, A.J.R. (2011) Revisiting the compositions and volatile contents of olivine-hosted melt inclusions from the Mount Shasta region: implications for the formation of high-Mg andesites. Contributions to Mineralogy and Petrology, 162, 109–132.

Schmidt, M.E., and Grunder, A.L. (2011) Deep Mafic Roots to Arc Volcanoes: Mafic Recharge and Differentiation of Basaltic Andesite at North Sister Volcano, Oregon Cascades. Journal of Petrology, 52, 603–641.

Schmidt, M.E., Grunder, A.L., and Rowe, M.C. (2008) Segmentation of the Cascade Arc as indicated by Sr and Nd isotopic variation among diverse primitive basalts. Earth and Planetary Science Letters, 266, 166–181.

Shaw, S. (2011) $H_2O$ contents in olivine-hosted melt inclusions from primitive magmas in the northern Cascade Arc, 76 p. M.S. thesis, Western Washington University, Bellingham.

Sisson, T.W., and Grove, T.L. (1993) Experimental investigations of the role of $H_2O$ in calc-alkaline differentiation and subduction zone magmatism. Contributions to Mineralogy and Petrology, 113, 143–166.

Sisson, T.W., Salters, V.J.M., and Larson, P.B. (2014) Petrogenesis of Mount Rainier andesite: Magma flux and geologic controls on the contrasting differentiation styles at stratovolcanoes of the southern Washington Cascades. Geological Society of America Bulletin, 126, 122–144.

Skulski, T., Minarik, W., and Watson, E.B. (1994) High-pressure experimental trace-element partitioning between clinopyroxene and basaltic melts. Chemical Geology, 117, 127–147.

Stern, C.R., and Kilian, R. (1996) Role of the subducted slab, mantle wedge and continental crust in the generation of adakites from the Andean Austral Volcanic Zone. Contributions to mineralogy and petrology, 123, 263–281.

Straub, S.M., LaGatta, A.B., Martin-Del Pozzo, A.L., and Langmuir, C.H. (2008) Evidence from high-Ni olivines for a hybridized peridotite/pyroxenite source for orogenic andesites from the central Mexican Volcanic Belt: andesite petrogenesis in Central MVB. Geochemistry, Geophysics, Geosystems, 9, Q030007.

Straub, S.M., Gomez-Tuena, A., Stuart, F.M., Zellmer, G.F., Espinasa-Perena, R., Cai, Y., and Iizuka, Y. (2011) Formation of hybrid arc andesites beneath thick continental crust. Earth and Planetary Science Letters, 303, 337–347.

Streck, M.J., Leeman, W.P., and Chesley, J. (2007) High-magnesian andesite from Mount Shasta: A product of magma mixing and contamination, not a primitive mantle melt. Geology, 35, 351–354.

Sun, S., and McDonough, W.F. (1989) Chemical and isotopic systematics of oceanic basalts: implications for mantle composition and processes. Geological Society Special Publications, 42, 313–345.

Syracuse, E.M., van Keken, P.E., and Abers, G.A. (2010) The global range of subduction zone thermal models. Physics of the Earth and Planetary Interiors, 183, 73–90.

Tabor, R.W., and Crowder, D.F. (1969) On batholiths and volcanoes: Intrusion and eruption of late Cenozoic magmas in the Glacier Peak area, North Cascades, Washington. U.S. Geological Survey Professional Paper 604, 67 p.

Tatsumi, Y., and Hanyu, T. (2003) Geochemical modeling of dehydration and partial melting of subducting lithosphere: Toward a comprehensive understanding of high-Mg andesite formation in the Setouchi volcanic belt, SW Japan. Geochemistry, Geophysics, Geosystems, 4, 1081.

Tatsumi, Y., Shukuno, H., Sato, K., Shibata, T., and Yoshikawa, M. (2003) The petrology and geochemistry of high-magnesium andesites at the western tip of the Setouchi Volcanic Belt, SW Japan. Journal of Petrology, 44, 1561–1578.

Taylor, D.D. (2001) Petrology and geochemistry of mafic lavas near Glacier Peak, North Cascades, Washington, M.S. thesis, Western Washington University, Bellingham.

Walowski, K.J., Wallace, P.J., Hauri, E.H., Wada, I., and Clynne, M.A. (2015) Slab melting beneath the Cascade Arc driven by dehydration of altered oceanic peridotite. Nature Geoscience, 8, 404–408.

Walowski, K.J., Wallace, P.J., Clynne, M.A., Rasmussen, D.J., and Weis, D. (2016) Slab melting and magma formation beneath the southern Cascade arc. Earth and Planetary Science Letters, 446, 100–112.

Wang, Z., and Gaetani, G.A. (2008) Partitioning of Ni between olivine and siliceous eclogite partial melt: experimental constraints on the mantle source of Hawaiian basalts. Contributions to Mineralogy and Petrology, 156, 661–678.

White, W.M., Hofmann, A.W., and Puchelt, H. (1987) Isotope geochemistry of Pacific mid-ocean ridge basalt. Journal of Geophysical Research, 92, 4881–4893.

Wilson, D.S. (1993) Confidence intervals for motion and deformation of the Juan de Fuca plate. Journal of Geophysical Research, 98, 16053–16071.

Yogodzinski, G.M., and Kelemen, P.B. (1998) Slab melting in the Aleutians: implications of an ion probe study of clinopyroxene in primitive adakite and basalt. Earth and Planetary Science Letters, 158, 53–65.

Yogodzinski, G.M., and Kelemen, P.B. (2007) Trace elements in clinopyroxenes from Aleutian xenoliths: Implications for primitive subduction magmatism in an island arc. Earth and Planetary Science Letters, 256, 617–632.

Yogodzinski, G.M., Kay, R.W., Volynets, O.N., Koloskov, A.V., and Kay, S.M. (1995) Magnesian andesite in the western Aleutian Komandorsky region: implications for slab melting and processes in the mantle wedge. Geological Society of America Bulletin, 107, 505–519.

Yogodzinski, G.M., Lees, J.M., Churikova, T.G., Dorendorf, F., Wöerner, G., and Volynets, O.N. (2001) Geochemical evidence for the melting of subducting oceanic lithosphere at plate edges. Nature, 409, 500–504.

**Figure 1.** Map of the Cascade Arc and associated subduction zone. Black and white triangles represent volcanic centers of interest and solid black triangles represent major volcanic centers. Dashed line shows the Guffanti and Weaver (1988) Garibaldi Volcanic Belt segment. Subduction rates are from McCrory et al. (2012) and Braunmiller and Nábělek (2002). Modified from Borg and Clynne (1998).

**Figure 2.** Graphical representation of olivine Fo contents; Fo = molar (Mg/(Mg+Fe))*100. TP: Tarn Plateau, GC: Glacier Creek, LC: Lightning Creek, M: mafic inclusion, I: intermediate inclusion. Asterisk (*) indicates EDS data. **a** Fo of analyzed olivine. **b** Fo of analyzed olivine relative to host rock Mg# with calculated equilibrium line. Olivine/liquid Fe-Mg partition coefficient uses estimated $Fe^{2+}_{liq}$ (Sisson and Grove 1993). Additional data from Taylor (2001), Baggerman and DeBari (2011), and Moore and DeBari (2012).

**Figure 3.** Graphical representation of Mg contents in clinopyroxene; Mg# = molar (Mg/(Mg+$Fe^{2+}$))*100. **a** Mg# of analyzed clinopyroxene. **b** Mg# of analyzed clinopyroxene relative to host rock Mg# with calculated equilibrium line. Clinopyroxene/liquid Fe-Mg partition coefficient uses calculated $Fe^{2+}_{liq}$=0.86 total $Fe_{liq}$ (Sisson and Grove 1993). Abbreviations, asterisk, and additional data are the same as Figure 2.

**Figure 4.** Graphical representation of An in plagioclase; An = (Ca/(Ca+Na+K))*100. Abbreviations, asterisk, and additional data are the same as Figure 2.

**Figure 5.** Olivine core Fo versus Ni contents (ppm). Pyroxenite and peridotite mantle source fields are from Straub et al. (2011). Tarn Plateau olivine is not in equilibrium with a mantle source, and low Ni contents in olivine are not consistent with fractionation from partial melts of a pyroxenite mantle. Glacier Creek olivine shows a trend (dashed line) that is similar to

olivine found in HMA and HMBA from the Mexican Volcanic Belt (Straub et al. 2008, 2011), but no mantle-equilibrium olivine has been preserved. Lightning Creek olivine is in equilibrium with a peridotite mantle.

**Figure 6.** Whole rock major element variation diagrams, with additional Cascade Arc data for comparison. CAB: calcalkaline basalt, HMA: high-Mg andesite, PMA: primitive magnesian andesite. Mount Baker CAB compositions are from Moore and DeBari (2012; Lake Shannon), Glacier Peak CAB compositions from Taylor (2001; Indian Pass), Mount Shasta data include Shastina, Sargents, and PMA compositions from Grove et al. (2002, 2005), Aleutian adakites compositions are from Yogodzinski and Kelemen (1998), Tonga boninites compositions are from Falloon et al. (2008). Mg# = $(Mg/(Mg+Fe^{2+}))*100$, with $Fe^{2+}$ calculated as 0.85 for Mount Baker rock units (Moore and DeBari 2012) and 0.80 for Glacier Peak rock units (Shaw 2011).

**Figure 7.** Whole rock trace element variation diagrams, with additional Cascade Arc data for comparison. Abbreviations and data are the same as Figure 6.

**Figure 8. a** Primitive mantle normalized whole rock trace element concentrations. **b – d** Chondrite normalized whole rock REE concentrations. Primitive mantle, chondrite, and N-MORB (normal mid-ocean ridge basalt) data from Sun and McDonough (1989). Mount Baker dacite composition is from Gross (2012) and Glacier Peak dacite composition is from DeBari et al. (in review). All other data are the same as Figure 6.

**Figure 9.** Whole rock isotopic compositions. **a** $\varepsilon_{Nd}$ versus $^{87}Sr/^{86}Sr$. **b** $^{207}Pb/^{204}Pb$ versus $^{206}Pb/^{204}Pb$. Tarn Plateau data are from Moore and DeBari (2012) and Mullen and McCallum

(2014). Lightning Creek data are from DeBari et al. (in review), and circles with dark outlines represent samples with gradual isotopic enrichment. Cascade CAB consist of calcalkaline basalts through andesites and is compiled from Tabor and Crowder (1969), Grove et al. (1988, 2002), Bullen and Clynne (1990), Leeman et al. (1990, 2004, 2005), Baker et al. (1991), Bacon et al. (1994, 1997), Borg et al. (1997), Green and Harry (1999), Conrey et al. (2001), Green and Sinha (2005), Magna et al. (2006), Schmidt et al. (2008), Jicha et al. (2009), Mitchell and Asmerom (2011), Schmidt and Grunder (2011), Moore and DeBari (2012), Mullen and Weis (2013), Mullen and McCallum (2014), and Sisson et al. (2014). Northern Hemisphere Reference Line (NHRL) is from Hart (1984), Juan de Fuca MORB compositions are from White et al. (1987). Compositional ranges for NE Pacific open ocean sediments and Cascadia continental derived sediments are from Church (1976). Cascadia bulk subducted sediment composition is from Plank and Langmuir (1998).

**Figure 10.** Chondrite normalized clinopyroxene REE abundances and variations in whole rock $SiO_2$. **a** Tarn Plateau clinopyroxene. **b** Glacier Creek clinopyroxene. **c** Lightning Creek clinopyroxene.

**Figure 11.** Clinopyroxene trace element contents and ratios versus Mg#. **a** Yb contents. **b** Chondrite normalized Nd/Yb contents. Lines represent $(Nd/Yb)_N$ of REE equilibrium clinopyroxene (REC) calculated using partition coefficients of Gaetani et al. (2003) for Tarn Plateau and Lightning Creek HMBA and Fujimaki et al. (1984) for Glacier Creek HMA. **c** Sr contents. Aleutian adakites data from Yogodzinski and Kelemen (1998). See text for explanation of REC.

**Figure 12.** BSE photomicrograph of a Tarn Plateau clinopyroxene grain from the high Mg# population, with an accompanying digitized image to highlight the positive relationship between Mg# and $(Nd/Yb)_N$ in different chemical zones. Circles represent EMP and LA-ICP-MS analysis location.

**Figure 13.** Chondrite-normalized REE patterns for clinopyroxene cores and rims, whole rock, and equilibrium liquid (REL) compositions calculated using clinopyroxene REE concentrations and partition coefficients described in Figure 11. See text for explanation of REL. White scale bars in images are 500 µm. Spots represent EMP and LA-ICP-MS analysis locations and their corresponding Mg#, with dark tones showing core analyses and light tones showing rim analyses. **a** Tarn Plateau clinopyroxene. **b** Glacier Creek clinopyroxene. **c** Lightning Creek clinopyroxene.

**Figure 14.** Whole rock primitive mantle-normalized Sr/P versus $SiO_2$ wt%. Dashed line represented $(Sr/P)_N$ boundary (3.3) between calcalkaline non-magnesian lavas and magnesian andesites from the Lassen Volcanic Center (Clynne and Borg 1997). Abbreviations and data are the same as Figure 5.

**Figure 15.** Fractional crystallization (**a – d**) and mass balance (**e – f**) models using primitive Mount Baker and Glacier Peak CAB as parental melts with a mineral assemblage of garnet (gnt), clinopyroxene (cpx), orthopyroxene (opx), and olivine (olv) ± hornblende (hbl). **a**, **c**, and **e** have a pyroxenite mineral assemblage (+hbl) and **b**, **d**, and **f** have a harzburgite mineral assemblage. Partition coefficients are listed in Table 5. Mineral compositions are from Müntener et al. (2001) and the adakites field is from Macpherson et al. (2006). Mount Baker

data are from Moore and DeBari (2012; Lake Shannon) and Glacier Peak data are from Taylor (2001; Indian Pass).

**Figure 16.** Simplified schematic showing petrogenetic interpretations for the three rock units. **a** Tarn Plateau HMBA: mixing between (1) a hydrous, LILE-rich, intermediate slab melt that interacted with the overlying mantle to become Mg-rich and (2) a differentiate of depleted mantle-derived basalt. **b** Glacier Creek HMA: (1) partial melt of the mantle that was hydrated by a LILE-rich slab component and underwent fractionation, mixing, and homogenization with (2) late-stage addition of a high-Ni olivine-bearing mantle-derived mafic component. **c** Lightning Creek HMBA: mixing between (1) partial melt of a depleted mantle that was hydrated by a LILE-rich slab component (mafic inclusion liquid), (2) a crustally-derived dacite (DeBari et al. in review), and (3) andesite that fractionated from mantle partial melts (intermediate inclusion liquid).

**Table 1** Petrographic summary

| Rock Unit | Phenocryst (%) | Phenocryst Modes | Mg# or An (cores) | Zoning | Size Range (mm) | Shape | Twinning | Disequilibrium Textures | Additional Observations |
|---|---|---|---|---|---|---|---|---|---|
| **MBVF** | | | | | | | | | |
| *Tarn Plateau HBMA* | 30-35 | Cpx (40-65%) | 88-94[1A]<br>73-79[2] | sec[1], rev[1&2],<br>norm[1] | 0.25-2.8[1]<br>0.25-2.0[2] | eu-sub | poly[1&2]<br>sim[1&2], osc[2] | Rounded cores (uncommon)[i], patchy to blebby cores (common), emb (rare)[2] | Composite crystals (common)[1&2], in clots (common)[1&2], Fe-rich cores[2] |
| | | Plag (25-45%) | 54-58[1 EDS]<br>83-88[2A] | norm[1&2], osc[2],<br>pat[1&2] | 0.5-4.9[1]<br>0.25-3.7[2] | eu-an | poly[1&2] | Fine siev[1], coarse siev[2], thin ovg rims[1&2], glass & pyroxene inclusions[1&2] | In clots with cpx (common)& olv (uncommon)[2] |
| | | Olv (10-20%) | 78-85 | norm | 0.25-2.9 | eu-an | -- | Emb, thin rxr | Fe & S inclusions (rare), Cr-ox (uncommon) |
| | | Opx (<3%) | 68-70[i] | rev | 0.5-1.0 | sub | -- | Ratty rxr (weak, uncommon) | |
| | | Groundmass: hypocrystalline (pyroxene granules, microlitic plag, Fe-Ti ox, abundant iddingsite | | | | | | | |
| *Glacier Creek HMA* | 20-25 | Plag (50-70%) | 43-58[1A]<br>43-54[2] | osc[1], norm[1&2],<br>rev[1&2] | 0.25-4[1]<br>0.3-1.3[2] | eu-an | poly[1&2] | Unsiev-coarse siev[1], ovg rims (thick[1], thin[2]) glass & pyroxene inclusions[1], fine siev[2] | In clots with cpx & opx[1&2] |
| | | Cpx (10-23%) | 76-80 | rev, pat | 0.25-2.0 | eu-an | sim, poly | Blebby, rxr (rare) | Composite crystals (rare) |
| | | Opx (10-20%) | 70-73[ii] | rev | 0.25-1.5 | eu-sub | -- | Emb, blebby inclusions | Tabular |
| | | Olv (3-7%) | 81-86[1]<br>71-77[2] | norm[1&2] | 0.5-2.0 | sub-an | -- | Emb[1&2], opx rxr (thin[1], thick[2]), ox inclusions[1&2] | Sparse Cr-ox[1&2], other ox[1&2], in monomineralic clots[1&2] |
| | | Groundmass: hypocrystalline (cpx granules, microlitic plag, abundant Fe-Ti ox, rare large (0.2-0.5 mm) and res xenocrystic Cr-ox | | | | | | | |
| **Glacier Peak** | | | | | | | | | |
| *Lightning Creek HMBA* | 20-30 | Plag (40-60%) | 48, 65-66[1A]<br>42-44[2A]<br>47-89[3] | osc[1&3] | 0.5-3.0[1]<br>0.25-2.4[2]<br>0.4-4.3[3] | eu-sub | poly[1-3] | Fine siev (core[1], rim[2]), coarse siev with solid core[3], pyroxene & glass inclusions[1-3], calcic ovg rims[2&3] | Distinct osc zoning[3], some in clots with twinned clinopyroxene[2], often elongate and tabular[2] |
| *Hybridized magmatic component* | | Cpx (20-30%) | 86-89[1]<br>80-84[2] | sec[1&2],<br>norm[1&2], rev[1&2] | 0.3-1.5[1&2] | eu-sub | sim[1&2]<br>poly[1&2] | Thin rxr[1&2], patchy cores (slight)[1&2] | Some composite[1&2], in clots with plag[2], grown around opx cores (uncommon) |
| | | Olv (15-20%) | 80, 89-91 | norm | 0.25-3.5 | eu-an | -- | Emb, thin opx rxr, ox inclusions | Cr-ox, other ox |
| | | Opx (5-10%) | 77-82[iv] | pat (weak) | 0.5-2 | eu-an | -- | Blebby (slight), res rims, glass inclusions | Some elongate, rare ox inclusions |
| | | Groundmass: hypocrystalline (dominantly microlitic plag up to 0.25 mm, Fe-Ti ox | | | | | | | |
| *Mafic inclusion* | 5-7 | Olv (75-85%) | 88-89 | norm | 0.25-1.1 | eu-sub | -- | Emb (weak), ox inclusions | Abundant Cr-ox |
| | | Cpx (15-25%) | 87[EDS] | -- | ≤0.5 | sub-an | -- | Ratty rims, ox inclusions (uncommon) | |
| | | Groundmass: holocrystalline (strongly zoned and abundant plag, clinopyroxene granules, some acicular ilm, rare apt | | | | | | | |
| *Intermediate inclusion* | 40-50 | Plag (70-80%) | 47 | osc<br>pat | 0.4-3.6 | eu-sub | poly<br>sim | Unsiev, patchy cores, cpx ox glass & apt inclusions, ratty rims (weak) and/or fine siev near rim (uncommon) | In clots with all other modes (common), tabular |
| | | Opx (10-15%) | 65-70[iv] | rev | 0.5-2.0 | eu-an | -- | Emb, large ox inclusions, cpx jackets (rare) | Some very elongate, in clots |
| | | Cpx (5-10%) | 75-80 | rev, pat (rare) | 0.25-1.0 | sub-an | sim (rare) | Emb, abundant ox inclusions | Large ox inc (≤180 µm), in clots |
| | | Olv (≤5%) | 78-82[EDS] | norm | ≤0.5 | an | -- | Opx rxr, ox inclusions | In clots with opx |
| | | Groundmass: hypocrystalline (abundant glass, microlitic plag, pyroxene granules, Fe-Ti ox, and bladed ilm | | | | | | | |

In cpx, Mg# = (Mg/(Mg+$Fe^{2+}$))*100; in olivine, Fo is the same as Mg# for cpx except Fe = $Fe^{Total}$; in plag, An = (Ca/(Ca+Na+K))*100. -- none observed

[1,2,3]each number represents a different populations (A: more abundant). If no number is given only one population was observed. [EDS]EDS qualitative analyses

Modes: *Olv:* olivine, *cpx:* clinopyroxene, *opx:* orthopyroxene, *plag:* plagioclase, *ox* : oxide, *ilm* : ilmenite, *apt* : apatite

Zoning: *norm:* normal, *rev:* reverse, *osc:* oscillatory, *sec:* sector, *pat:* patchy Twinning: *poly:* polysynthetic, *sim:* simple

Textures: *emb:* embayed, *rxr:* reaction rims, *res:* resorbed, *siev:* seived, *ovg:* overgrowth Shape: eu: euhedral, sub: subhedral, an: andehral

[i]Data from Moore & DeBari (2012), [ii]Partial data from Baggerman & DeBari (2011), [iii]Partial data from Taylor (2001)

**Table 2** Representative clinopyroxene trace element concentrations (ppm) determined using LA-ICP-MS

| Label | L | Sr | La | Ce | Nd | Sm | Eu | Gd | Tb | Dy | Ho | Er | Tm | Yb | Lu |
|---|---|---|---|---|---|---|---|---|---|---|---|---|---|---|---|
| *Tarn Plateau HMBA* | | | | | | | | | | | | | | | |
| 2_2_2 | m | 44 | 0.4 | 2.0 | 3.2 | 1.1 | 0.4 | 1.4 | 0.2 | 1.5 | 0.3 | 0.9 | 0.1 | 0.6 | 0.1 |
| 2_2_3 | m | 46 | 1.0 | 5.1 | 6.2 | 2.4 | 0.7 | 2.6 | 0.4 | 2.9 | 0.6 | 1.5 | 0.2 | 1.4 | 0.2 |
| 2_2_4 | r | 51 | 0.8 | 3.8 | 5.0 | 1.8 | 0.5 | 2.1 | 0.3 | 2.0 | 0.4 | 1.0 | 0.1 | 0.9 | 0.2 |
| 2_3_1 | c | 63 | 0.3 | 2.3 | 3.0 | 1.1 | 0.3 | 1.1 | 0.1 | 0.9 | 0.2 | 0.4 | 0.0 | 0.3 | -- |
| 2_3_2 | m | 74 | 0.4 | 2.0 | 2.9 | 0.7 | 0.3 | 0.9 | 0.1 | 0.8 | 0.1 | 0.4 | 0.1 | 0.3 | 0.1 |
| 2_3_3 | m | 69 | 0.3 | 1.7 | 2.4 | 0.6 | 0.3 | 0.9 | 0.1 | 0.8 | 0.1 | 0.5 | 0.0 | 0.4 | 0.0 |
| 2_3_4 | r | 63 | 0.4 | 1.8 | 2.6 | 0.9 | 0.4 | 1.1 | 0.2 | 1.1 | 0.2 | 0.5 | 0.0 | 0.4 | 0.1 |
| 3_2_1 | c | 36 | 2.1 | 9.7 | 12.1 | 4.9 | 1.1 | 6.1 | 1.0 | 6.2 | 1.3 | 3.7 | 0.5 | 3.0 | 0.4 |
| 3_2_2 | c | 39 | 1.5 | 7.0 | 9.4 | 3.0 | 0.9 | 4.3 | 0.7 | 4.7 | 1.0 | 2.1 | 0.4 | 2.2 | 0.3 |
| 3_2_3 | m | 34 | 1.7 | 7.5 | 9.5 | 3.5 | 1.0 | 4.5 | 0.7 | 5.0 | 0.9 | 2.8 | 0.3 | 2.1 | 0.3 |
| 3_2_4 | m | 36 | 1.2 | 5.2 | 6.9 | 2.5 | 0.7 | 2.9 | 0.5 | 3.2 | 0.7 | 2.0 | 0.3 | 1.9 | 0.3 |
| 3_2_5 | r | 36 | 1.9 | 8.3 | 10.4 | 4.0 | 1.1 | 5.3 | 0.9 | 5.3 | 1.0 | 3.1 | 0.5 | 2.4 | 0.3 |
| 3_5_1 | c | 45 | 0.8 | 4.0 | 5.0 | 2.0 | 0.6 | 2.5 | 0.4 | 2.4 | 0.5 | 1.5 | 0.2 | 1.0 | 0.2 |
| 3_5_2 | m | 49 | 0.9 | 4.1 | 5.3 | 1.9 | 0.6 | 2.3 | 0.4 | 2.4 | 0.5 | 1.3 | 0.2 | 1.1 | 0.2 |
| 3_5_3 | m | 57 | 0.9 | 4.0 | 5.1 | 1.9 | 0.6 | 1.9 | 0.3 | 2.2 | 0.4 | 1.2 | 0.2 | 0.9 | 0.1 |
| 3_5_4 | r | 63 | 0.9 | 4.6 | 6.1 | 1.9 | 0.7 | 2.3 | 0.4 | 2.2 | 0.4 | 1.1 | 0.1 | 1.1 | 0.1 |
| 4_3_1 | c | 68 | 0.8 | 4.2 | 5.4 | 1.8 | 0.6 | 2.0 | 0.3 | 2.2 | 0.4 | 1.2 | 0.2 | 0.8 | 0.1 |
| 4_3_2 | m | 70 | 0.4 | 2.2 | 2.5 | 1.0 | 0.3 | 1.2 | 0.1 | 1.1 | 0.2 | 0.6 | 0.1 | 0.3 | 0.0 |
| 4_3_3 | m | 87 | 0.7 | 3.0 | 3.6 | 1.4 | 0.3 | 1.0 | 0.2 | 1.0 | 0.2 | 0.6 | 0.1 | 0.3 | 0.1 |
| 4_3_4 | r | 66 | 1.0 | 4.7 | 6.6 | 2.2 | 0.7 | 2.7 | 0.4 | 2.4 | 0.6 | 1.3 | 0.2 | 1.2 | 0.2 |
| 4_3_5 | m | 88 | 0.7 | 3.2 | 4.2 | 1.1 | 0.5 | 1.6 | 0.2 | 1.2 | 0.2 | 0.4 | 0.1 | 0.4 | 0.1 |
| 4_4_1 | c | 36 | 2.3 | 10.6 | 13.7 | 4.8 | 1.1 | 7.1 | 1.0 | 6.7 | 1.3 | 4.4 | 0.5 | 4.0 | 0.5 |
| 4_4_3 | m | 57 | 1.6 | 7.1 | 9.3 | 3.2 | 0.8 | 3.4 | 0.5 | 3.0 | 0.6 | 2.0 | 0.3 | 1.7 | 0.2 |
| 4_4_4 | r | 57 | 0.9 | 4.3 | 5.3 | 1.9 | 0.6 | 2.7 | 0.4 | 2.1 | 0.4 | 1.1 | 0.2 | 0.8 | 0.1 |
| 4_4_5 | c | 35 | 2.5 | 10.9 | 13.4 | 4.9 | 1.2 | 6.1 | 1.0 | 6.6 | 1.3 | 3.8 | 0.6 | 3.1 | 0.5 |
| 6_3_2 | m | 68 | 1.1 | 4.6 | 5.7 | 2.1 | 0.8 | 2.4 | 0.4 | 2.5 | 0.5 | 1.4 | 0.2 | 1.1 | 0.1 |
| 6_3_3 | r | 65 | 1.2 | 5.4 | 6.7 | 2.9 | 0.8 | 2.9 | 0.4 | 3.2 | 0.5 | 1.6 | 0.2 | 1.4 | 0.2 |
| *Glacier Creek HMA* | | | | | | | | | | | | | | | |
| 5_1_1 | c | 36 | 3.7 | 14.5 | 16.8 | 6.4 | 1.3 | 6.3 | 1.0 | 7.4 | 1.4 | 3.6 | 0.5 | 3.7 | 0.4 |
| 5_1_2 | m | 39 | 4.6 | 19.5 | 20.5 | 7.1 | 1.3 | 7.8 | 1.2 | 8.6 | 1.7 | 4.6 | 0.6 | 4.3 | 0.6 |
| 5_1_3 | r | 43 | 2.1 | 9.2 | 11.7 | 3.5 | 1.1 | 4.3 | 0.8 | 4.9 | 0.9 | 2.7 | 0.3 | 2.2 | 0.3 |
| 5_1_4 | r | 34 | 4.5 | 20.3 | 23.4 | 8.6 | 1.5 | 10.3 | 1.6 | 10.4 | 2.1 | 6.7 | 0.9 | 5.4 | 0.8 |
| 5_3_1 | c | 34 | 3.6 | 15.3 | 19.5 | 6.4 | 1.4 | 7.8 | 1.4 | 8.6 | 1.8 | 5.3 | 0.7 | 4.4 | 0.7 |
| 5_3_2 | m | 37 | 4.1 | 18.0 | 23.4 | 8.1 | 1.5 | 9.3 | 1.6 | 9.9 | 2.0 | 5.8 | 0.8 | 4.9 | 0.7 |
| 7_1_2 | r | 51 | 2.1 | 10.0 | 12.1 | 4.1 | 1.2 | 5.1 | 0.8 | 5.0 | 0.8 | 2.8 | 0.4 | 2.3 | 0.3 |
| 7_1_3 | m | 35 | 4.3 | 19.2 | 23.9 | 7.6 | 1.4 | 9.0 | 1.5 | 10.2 | 2.3 | 5.7 | 0.8 | 5.3 | 0.8 |
| 7_3_1 | c | 33 | 2.9 | 13.1 | 16.5 | 5.6 | 1.2 | 6.7 | 1.2 | 7.0 | 1.4 | 4.0 | 0.6 | 3.9 | 0.6 |
| 7_3_2 | c | 28 | 3.4 | 16.0 | 19.7 | 6.7 | 1.3 | 8.7 | 1.5 | 9.2 | 1.9 | 5.4 | 0.7 | 4.4 | 0.6 |
| 7_3_3 | r | 33 | 2.4 | 12.0 | 15.0 | 5.4 | 1.2 | 6.4 | 1.0 | 7.0 | 1.4 | 4.0 | 0.5 | 3.6 | 0.5 |
| 7_3_4 | r | 35 | 1.6 | 6.9 | 8.5 | 3.2 | 0.8 | 4.2 | 0.6 | 3.5 | 0.7 | 2.0 | 0.3 | 1.9 | 0.2 |
| 12_5_1 | c | 39 | 2.9 | 12.3 | 15.8 | 4.9 | 1.2 | 6.6 | 1.1 | 6.4 | 1.3 | 3.5 | 0.5 | 3.6 | 0.5 |
| 12_5_2 | c | 43 | 3.9 | 16.9 | 18.9 | 6.7 | 1.4 | 7.7 | 1.2 | 7.9 | 1.6 | 5.0 | 0.6 | 4.1 | 0.5 |
| 12_5_3 | c | 36 | 3.3 | 14.4 | 17.3 | 6.5 | 1.4 | 6.7 | 1.2 | 8.6 | 1.5 | 4.3 | 0.6 | 3.8 | 0.6 |
| 12_5_4 | r | 33 | 4.0 | 17.2 | 20.6 | 6.9 | 1.2 | 8.2 | 1.2 | 8.6 | 1.7 | 5.0 | 0.6 | 4.3 | 0.8 |
| *Lightning Creek HMBA* | | | | | | | | | | | | | | | |
| 1_3_2 | m | 52 | 2.4 | 12.0 | 14.8 | 4.9 | 1.4 | 5.6 | 0.7 | 5.0 | 0.8 | 2.3 | 0.3 | 1.8 | 0.3 |
| 1_3_3 | r | 48 | 2.0 | 9.9 | 10.8 | 2.7 | 1.2 | 4.3 | 0.6 | 3.8 | 0.8 | 2.2 | 0.3 | 1.7 | 0.2 |
| 2_1_2 I | m | 35 | 2.8 | 12.2 | 15.2 | 4.6 | 1.1 | 6.0 | 0.8 | 5.2 | 0.9 | 2.9 | 0.4 | 2.0 | 0.3 |
| 2_1_3 I | r | 60 | 1.8 | 9.0 | 10.8 | 3.4 | 1.2 | 3.4 | 0.6 | 3.2 | 0.6 | 2.1 | 0.3 | 1.5 | 0.2 |
| 2_5_1 | c | 58 | 2.4 | 11.0 | 12.6 | 4.3 | 1.1 | 4.6 | 0.6 | 3.8 | 0.8 | 2.1 | 0.3 | 1.4 | 0.2 |
| 2_5_2 | m | 54 | 2.6 | 12.2 | 16.2 | 5.2 | 1.3 | 5.5 | 0.8 | 4.5 | 1.0 | 2.7 | 0.3 | 2.1 | 0.3 |
| 2_5_3 | r | 63 | 1.7 | 7.7 | 9.9 | 3.3 | 0.9 | 3.1 | 0.5 | 3.5 | 0.6 | 1.7 | 0.2 | 1.3 | 0.2 |
| 6_3_2 I | m | 25 | 5.3 | 24.6 | 29.3 | 10.1 | 1.5 | 12.2 | 1.9 | 13.0 | 2.6 | 7.5 | 1.0 | 6.4 | 0.9 |
| 12_2_2 | m | 58 | 2.1 | 10.3 | 14.4 | 4.1 | 1.1 | 4.1 | 0.6 | 3.2 | 0.6 | 2.0 | 0.2 | 1.4 | 0.2 |
| 12_2_3 | m | 35 | 2.0 | 8.6 | 11.1 | 3.8 | 1.1 | 3.9 | 0.6 | 3.7 | 0.8 | 2.0 | 0.3 | 1.6 | 0.2 |
| 12_2_4 | r | 56 | 2.6 | 11.0 | 13.7 | 5.0 | 1.3 | 5.5 | 0.6 | 3.9 | 0.9 | 2.2 | 0.3 | 2.2 | 0.3 |
| 12_4_2 | m | 57 | 2.1 | 9.2 | 11.0 | 3.6 | 1.0 | 3.6 | 0.5 | 3.2 | 0.6 | 1.6 | 0.2 | 1.2 | 0.2 |
| 12_4_3 | m | 44 | 1.8 | 8.8 | 11.2 | 3.6 | 1.1 | 3.5 | 0.6 | 3.6 | 0.6 | 1.8 | 0.2 | 1.6 | 0.2 |

L: locality of analysis spot (*c* : core, *m* : mid, *r* : rim). Labels are as follows: sample#_clinopyroxene#_analysis#. For example, 2_1_1 represents sample 2, clinopyroxene #1, analysis #1.

I: pyroxene crystals from the Lightning Creek intermediate inclusion.

Analyses were done at Western Washington University.

**Table 3** Lightning Creek whole rock major, minor and trace element compositions

| Sample | **LC-6H** | **LC-6M** | **LC-6I** | | **LC-6H** | **LC-6M** | **LC-6I** |
|---|---|---|---|---|---|---|---|
| *Major elements (wt. %)* | | | | *Trace elements by ICP-MS (ppm)* | | | |
| $SiO_2$ | 55.61 | 54.57 | 57.27 | La | 19.0 | 21.3 | 18.9 |
| $TiO_2$ | 0.94 | 1.15 | 1.22 | Ce | 43.3 | 50.4 | 42.7 |
| $Al_2O_3$ | 16.36 | 16.40 | 17.06 | Pr | 5.66 | 6.66 | 5.56 |
| FeO* | 5.93 | 6.73 | 6.73 | Nd | 22.8 | 26.8 | 22.7 |
| MnO | 0.11 | 0.12 | 0.12 | Sm | 4.55 | 5.22 | 4.84 |
| MgO | 6.23 | 7.74 | 4.79 | Eu | 1.40 | 1.57 | 1.51 |
| CaO | 7.72 | 8.82 | 6.49 | Gd | 3.83 | 4.36 | 4.45 |
| $Na_2O$ | 3.58 | 3.42 | 3.87 | Tb | 0.60 | 0.66 | 0.71 |
| $K_2O$ | 1.13 | 0.81 | 1.28 | Dy | 3.42 | 3.79 | 4.22 |
| $P_2O_5$ | 0.23 | 0.28 | 0.33 | Ho | 0.71 | 0.75 | 0.85 |
| Total | 97.85 | 100.03 | 99.15 | Er | 1.87 | 2.01 | 2.29 |
| Mg# | 69.8 | 71.7 | 61.0 | Tm | 0.26 | 0.28 | 0.34 |
| | | | | Yb | 1.64 | 1.73 | 2.08 |
| *Trace elements by XRF (ppm)* | | | | Lu | 0.26 | 0.27 | 0.33 |
| Ni | 101 | 135 | 64 | Ba | 375 | 323 | 383 |
| Cr | 205 | 292 | 109 | Th | 3.34 | 2.84 | 3.53 |
| Sc | 20 | 25 | 16 | Nb | 3.90 | 3.88 | 5.17 |
| V | 138 | 165 | 136 | Y | 17.4 | 18.8 | 21.4 |
| Ba | 384 | 331 | 381 | Hf | 3.78 | 4.19 | 4.29 |
| Rb | 20 | 15 | 23 | Ta | 0.32 | 0.30 | 0.42 |
| Sr | 781 | 928 | 596 | U | 1.11 | 0.88 | 1.17 |
| Zr | 155 | 169 | 192 | Pb | 5.06 | 4.06 | 6.21 |
| Y | 18 | 19 | 22 | Rb | 18.3 | 12.3 | 21.0 |
| Nb | 5.2 | 4.4 | 5.9 | Cs | 0.67 | 0.38 | 0.81 |
| Ga | 17 | 17 | 16 | Sr | 776 | 934 | 609 |
| Cu | 39 | 35 | 61 | Sc | 20.9 | 24.0 | 16.0 |
| Zn | 64 | 64 | 70 | Zr | 147 | 163 | 188 |
| Pb | 4.2 | 4.2 | 6.7 | | | | |
| La | 19 | 22 | 19 | | | | |
| Ce | 42 | 52 | 45 | | | | |
| Th | 3.7 | 3.8 | 4.0 | | | | |
| Nd | 21 | 25 | 23 | | | | |
| U | 1.6 | 2.9 | 2.9 | | | | |

All Fe is reported as FeO*. Mg# = $(Mg/(Mg+Fe^{2+}))*100$, where $Fe^{2+}/Fe^{1} = 0.80$, based on Shaw (2011).

*H* : hybridized magmatic component, *M* : mafic inclusion, *I* : intermediate inclusion.

Analyses were done at Washington State University GeoAnalytical Lab.

**Table 4** Glacier Creek Sr, Nd, and Pb isotopic compositions

| | GC-7 | GC-7 (2nd) |
|---|---|---|
| $^{87}Sr/^{86}Sr$ | 0.703267 | -- |
| $\varepsilon_{Sr}$ | -17.5 | -- |
| $^{143}Nd/^{144}Nd$ | 0.512972 | -- |
| $\varepsilon_{Nd}$ | 6.5 | -- |
| $^{206}Pb/^{204}Pb$ | 18.801 | 18.799 |
| $^{207}Pb/^{204}Pb$ | 15.549 | 15.548 |
| $^{208}Pb/^{204}Pb$ | 38.279 | 38.276 |
| $SiO_2$* | 58.51 | 58.51 |

Analyses were done at the University of Washington.
2σ errors for Sr and Nd are ± 40 and ± 30 ppm, or ± 0.4 and ± 0.3 epsilon units, respectively. 2σ errors for Pb are up to ± 200 ppm, or ± 0.02%.
(2nd): a repeat Pb analysis of the dissolved sample.
*Data from Baggerman & Debari (2011).

**Table 5** Mineral/liquid partition coefficients (Kds)

| | **Garnet[1]** | **Clinopyroxene[1]** | **Orthopyroxene[2]** | **Olivine[2]** | **Hornblende[3]** |
|---|---|---|---|---|---|
| La | | 0.09 | 0.0005 | 0.00005 | 0.2 |
| Ce | 0.01 | 0.13 | 0.003 | 0.00006 | 0.3 |
| Pr | *0.04* | *0.195* | *0.005* | *0.00013* | *0.5* |
| Nd | 0.071 | 0.26 | 0.007 | 0.0002 | 0.8 |
| Sm | 0.34 | 0.38 | 0.01 | 0.0006 | 1.1 |
| Eu | 0.44 | 0.24 | 0.013 | 0.00015 | 1.3 |
| Gd | *1* | *0.34* | 0.016 | 0.00099 | 1.8 |
| Tb | *2.5* | *0.47* | 0.021 | 0.002 | *1.9* |
| Dy | 3.2 | 0.57 | 0.025 | 0.004 | 2 |
| Ho | *3.8* | *0.58* | 0.029 | 0.002 | *2* |
| Er | 5 | 0.59 | 0.041 | 0.0087 | 1.9 |
| Yb | 7.4 | 0.61 | 0.047 | 0.017 | 1.7 |
| Lu | *8.2* | *0.68* | 0.052 | 0.02 | 1.5 |
| Y | 4.1 | 0.55 | 0.025 | 0.007 | 0.19 |
| Sr | 0.006 | 0.15 | 0.009 | 0.008 | 0.36 |

[1]Gaetani et al (2003) for hydrous peridotite.

[2]Donnelly et al (2004) for mid-ocean ridge basalt (MORB).

[3]Sen and Dunn (1994) for amphibolite.

*Italics* : interpolated

**Table 6** Mafic minerals pressure and temperature crystallization conditions

| | Temperature (°C) | Pressure (kbar) |
|---|---|---|
| ***Clinopyroxene & liquid thermobarometery (eql Kd = 0.27 ± 0.05)*** | | |
| *Tarn Plateau HMBA* | | |
| *High Mg# &* | 1,191 – 1,213(87)[32d] | 8.3 – 10.0(3.6)[31[3.4]] |
| *high Nd/Yb mafic liquid* | 1,119 – 1,135(42)[33[3.4]] | 9.4 – 10.7(5.0)[32c[3.4]] |
| *(4 eql clinopyroxene)* | 1,087 – 1,102(42)[33[5.8]] | 9.3 – 11.0(3.6)[31[5.8]] |
| | | 11.0 – 12.4(5.0)[32c[5.8]] |
| ***Orthopyroxene & clinopyroxene thermobarometry (eql Kd = 1.09 ± 0.14)*** | | |
| *Glacier Creek HMA* | | |
| *Intermediate liquid* | 1,014(56)[36+38] | 4.1 – 4.4(3.7)[38] |
| *(2 eql pairs)* | 1,009 – 1,010(56)[36+39] | 3.1 – 3.4(2.8)[39+36] |
| *Lightning Creek HMBA* | | |
| *Hybridized magmatic* | 1,004 – 1,032(56)[36+38] | 2.4 – 3.1(3.7)[38] |
| *component* | 999 – 1,034(56)[36+39] | 1.6 – 3.5(2.8)[39+36] |
| *(3 eql pairs)* | | |
| ***Olivine & liquid thermometry (eql Kd = 0.28 ± 0.03) and Silica activity barometry*** | | |
| *Lightning Creek HMBA* | | |
| *Mafic inclusion* | 1,207(51)[14] | 5.9(2.9)[42] |
| *(2 eql olivine)* | 1,192 – 1,193(43)[22+42] | 6.0(2.9)[42+22] |

*eql* : equilibrium

Parentheses by results indicate model error. For example, (1) reads as ± 1 °C or kbar.

[number] indicates the equation(s) used from Putirka (2008).

[number] $H_2O$ contents used in calculations. 5.8 wt% was calculated using Mitchell and Grove (2015; Table 7), 3.4 wt% is from Mullen and McCallum (2014).

Any Tarn Plateau whole rock data used in calculations is from Moore and DeBari (2012).

**Table 7** Calculated whole rock $H_2O$ contents and temperatures

| | Temperature (°C)[1] | $H_2O$ (wt%)[1] | $H_2O$ (wt%)[2] | $H_2O$ (wt%)[3] |
|---|---|---|---|---|
| *Tarn Plateau HMBA* | | | | |
| *TP-3* [i] | 1046 | 5.9 | 3.1 | ~4 |
| *TP-6* [i] | 1055 | 5.8 | 2.6 | ~2.5 |
| *02-MB-5* [ii] | 1042 | 6.0 | -- | -- |
| *Glacier Creek HMA* | | | | |
| *GC-5* [iii] | -- | -- | 1.6 | ~1 |
| *GC-7* [iii] | -- | -- | 2.0 | ~1 |
| *GC-12* [iii] | -- | -- | 2.4 | ~2 |
| *Lightning Creek HMBA* | | | | |
| *LC-1* [iv] | 1016 | 2.9 | 2.2 | ~2 |
| *LC-2* [iv] | 1029 | 2.7 | 2.1 | ~2 |
| *LC-4* [iv*] | 1024 | 2.9 | -- | -- |
| *LC-6* [iv] | 1045 | 2.4 | 1.5 | ~1 |
| *LC-12* [iv] | 1047 | 2.3 | 2.0 | ~1.5 |
| *LC-6M** | 1068 | 4.3 | -- | -- |

Pressures used for all calculations are minimum values from Table 6.

[1]Mitchell and Grove (2015) primitive andesites model (Glacier Creek samples not suitable); mean average error for this model is ± 1.4 wt% $H_2O$ and ± 23°C.

[2]Lange et al. (2009) plagioclase-liquid hygrometer; standard error of estimate for this model is ± 0.32 wt% $H_2O$.

[3]Sisson and Grove (1993) plagioclase-liquid Ca-Na exchange model. Outputs are graphical estimates.

*No plagioclase data available.

[i]whole rock data from Moore and DeBari (2012).

[ii]whole rock data from Mullen and McCallum (2014).

[iii]whole rock data from Baggerman and DeBari (2011).

[iv]whole rock data from Taylor (2001).

This is a preprint, the final version is subject to change, of the American Mineralogist (MSA)
Cite as Authors (Year) Title. American Mineralogist, in press.
(DOI will not work until issue is live.) DOI: http://dx.doi.org/10.2138/am-2017-5756

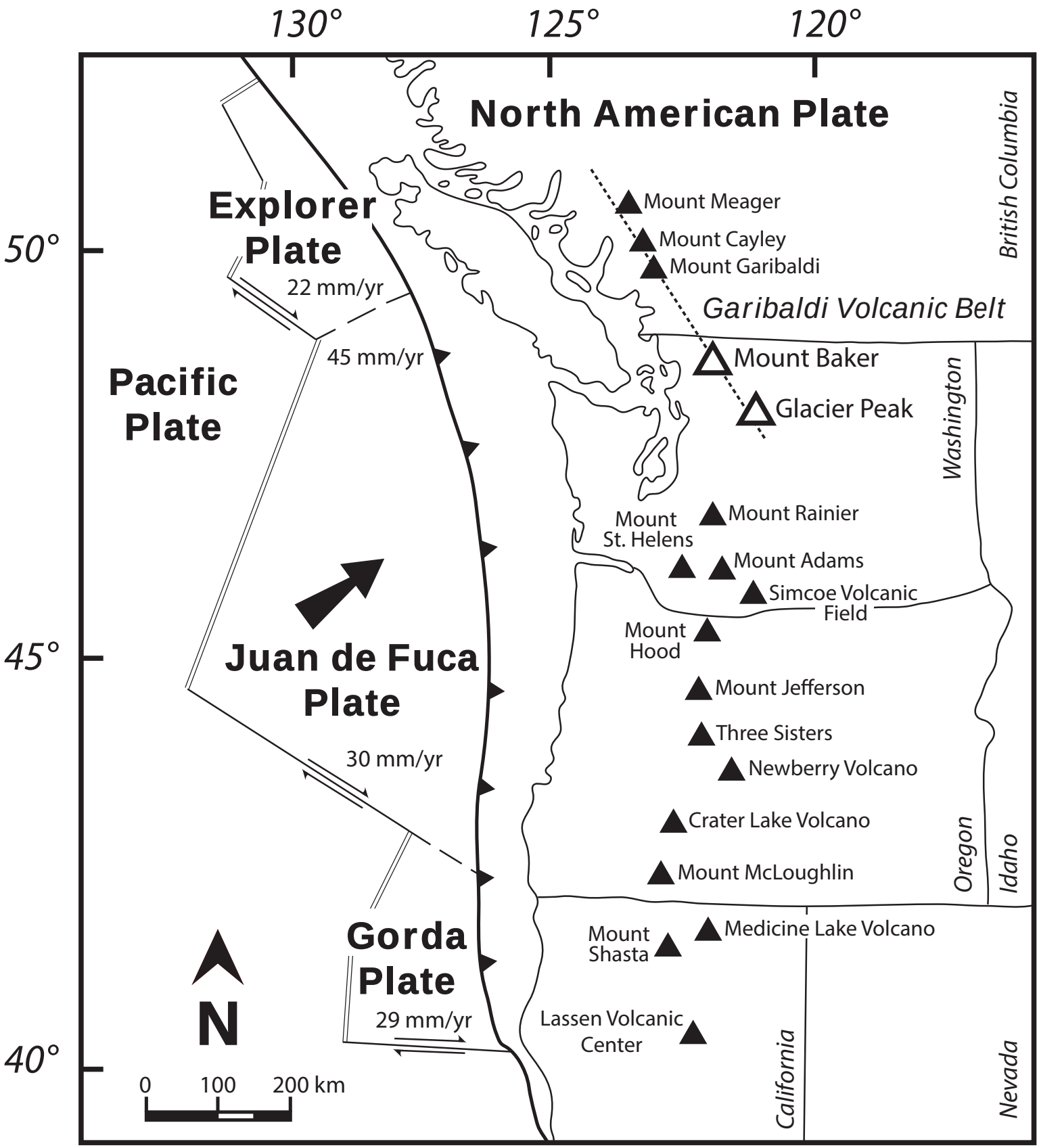


Figure 1

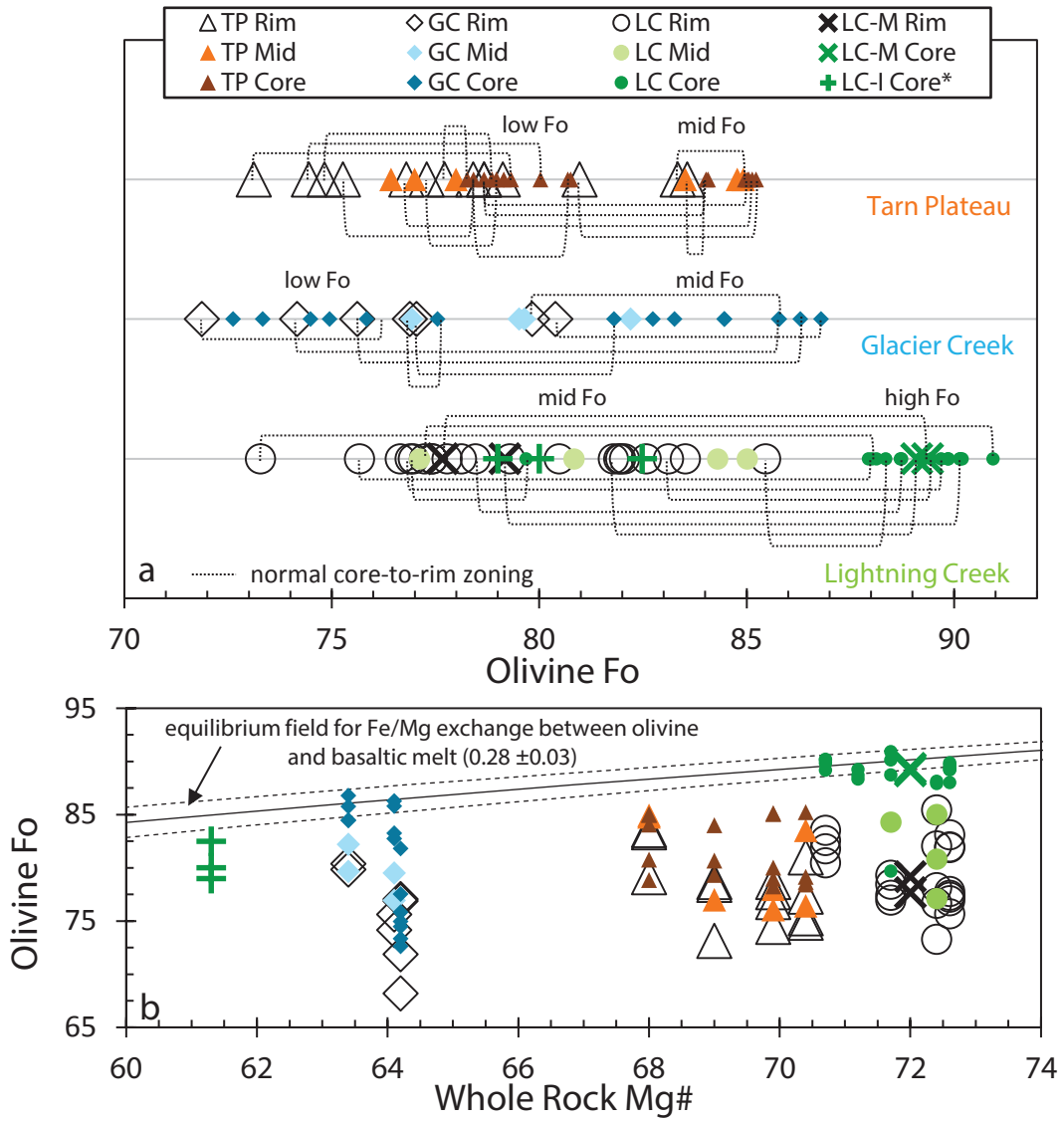
TP Rim
TP Mid
TP Core
GC Rim
GC Mid
GC Core
LC Rim
LC Mid
LC Core
LC-M Rim
LC-M Core
LC-I Core*
low Fo
mid Fo
Tarn Plateau
low Fo
mid Fo
Glacier Creek
mid Fo
high Fo
a
normal core-to-rim zoning
Lightning Creek
70
75
80
85
90
Olivine Fo
95
85
75
65
Olivine Fo
equilibrium field for Fe/Mg exchange between olivine
and basaltic melt (0.28 ±0.03)
b
60
62
64
66
68
70
72
74
Whole Rock Mg#

Figure 2

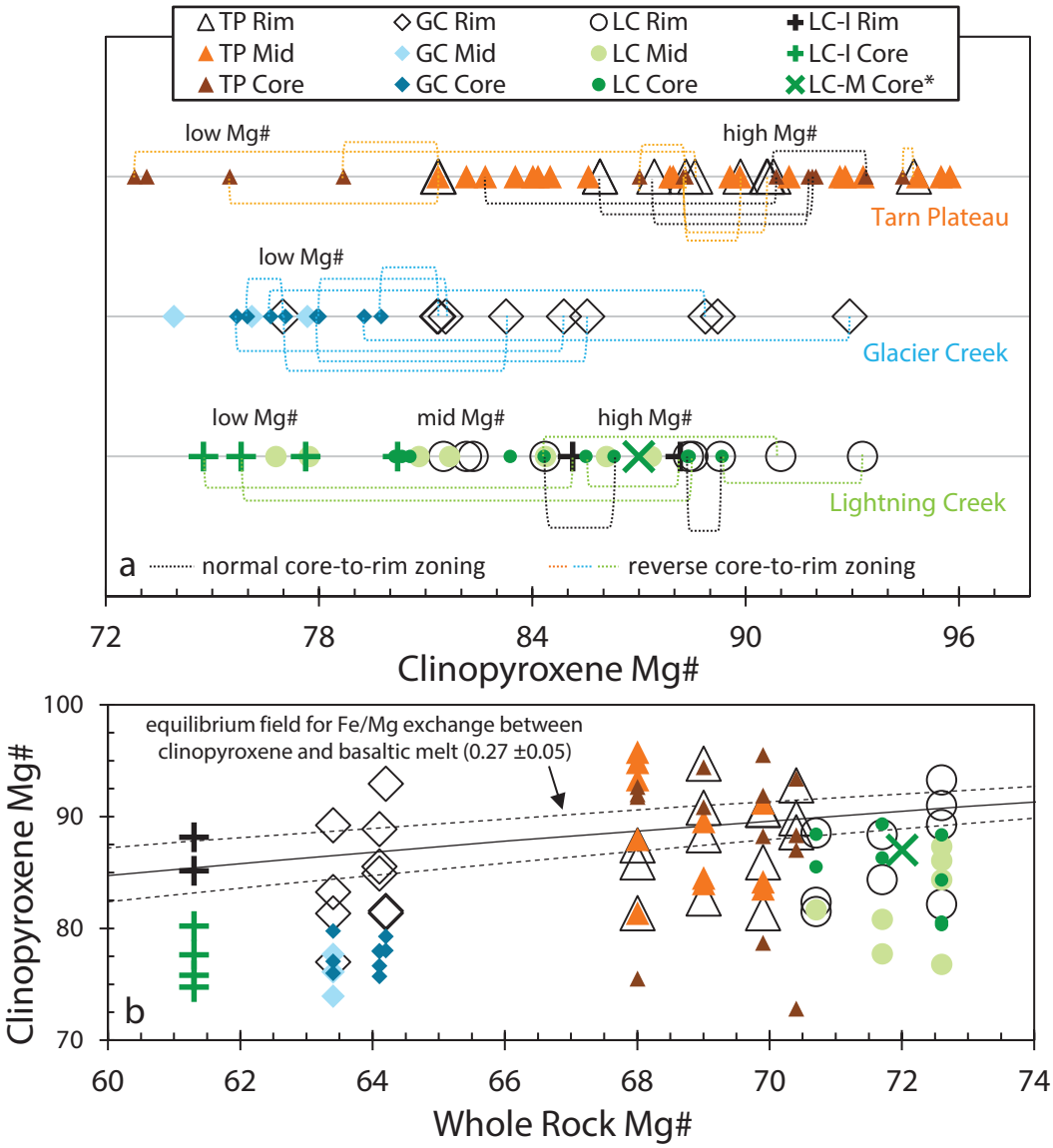
TP Rim
TP Mid
TP Core
GC Rim
GC Mid
GC Core
LC Rim
LC Mid
LC Core
LC-I Rim
LC-I Core
LC-M Core*
low Mg#
high Mg#
Tarn Plateau
low Mg#
Glacier Creek
low Mg#
mid Mg#
high Mg#
Lightning Creek
a
normal core-to-rim zoning
reverse core-to-rim zoning
72
78
84
90
96
Clinopyroxene Mg#
equilibrium field for Fe/Mg exchange between
clinopyroxene and basaltic melt (0.27 ±0.05)
Clinopyroxene Mg#
100
90
80
70
b
60
62
64
66
68
70
72
74
Whole Rock Mg#

Figure 3

This is a preprint, the final version is subject to change, of the American Mineralogist (MSA)
Cite as Authors (Year) Title. American Mineralogist, in press.
(DOI will not work until issue is live.) DOI: http://dx.doi.org/10.2138/am-2017-5756

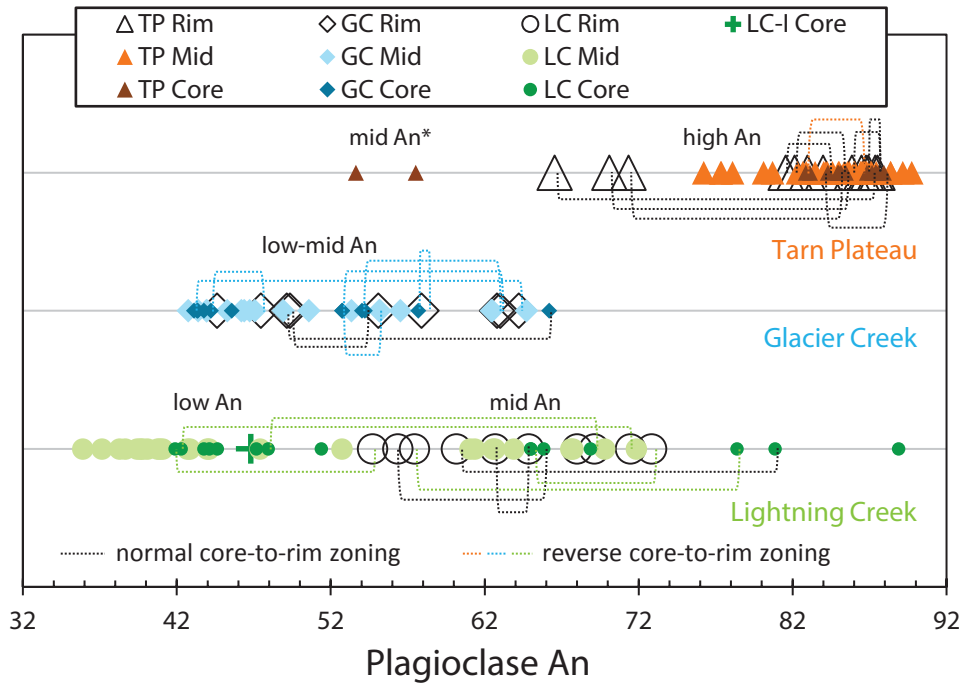


Figure 4

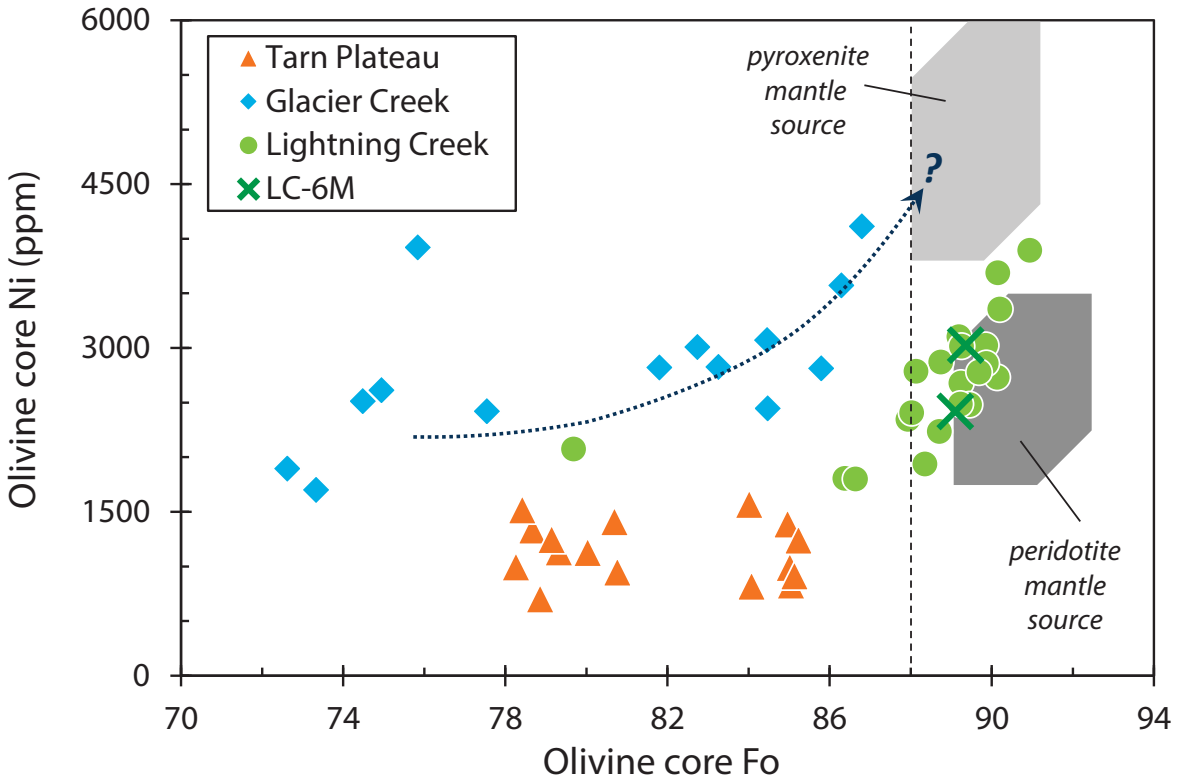
Tarn Plateau
Glacier Creek
Lightning Creek
LC-6M
pyroxenite mantle source
?
peridotite mantle source
Olivine core Ni (ppm)
Olivine core Fo
6000
4500
3000
1500
0
70
74
78
82
86
90
94

Figure 5

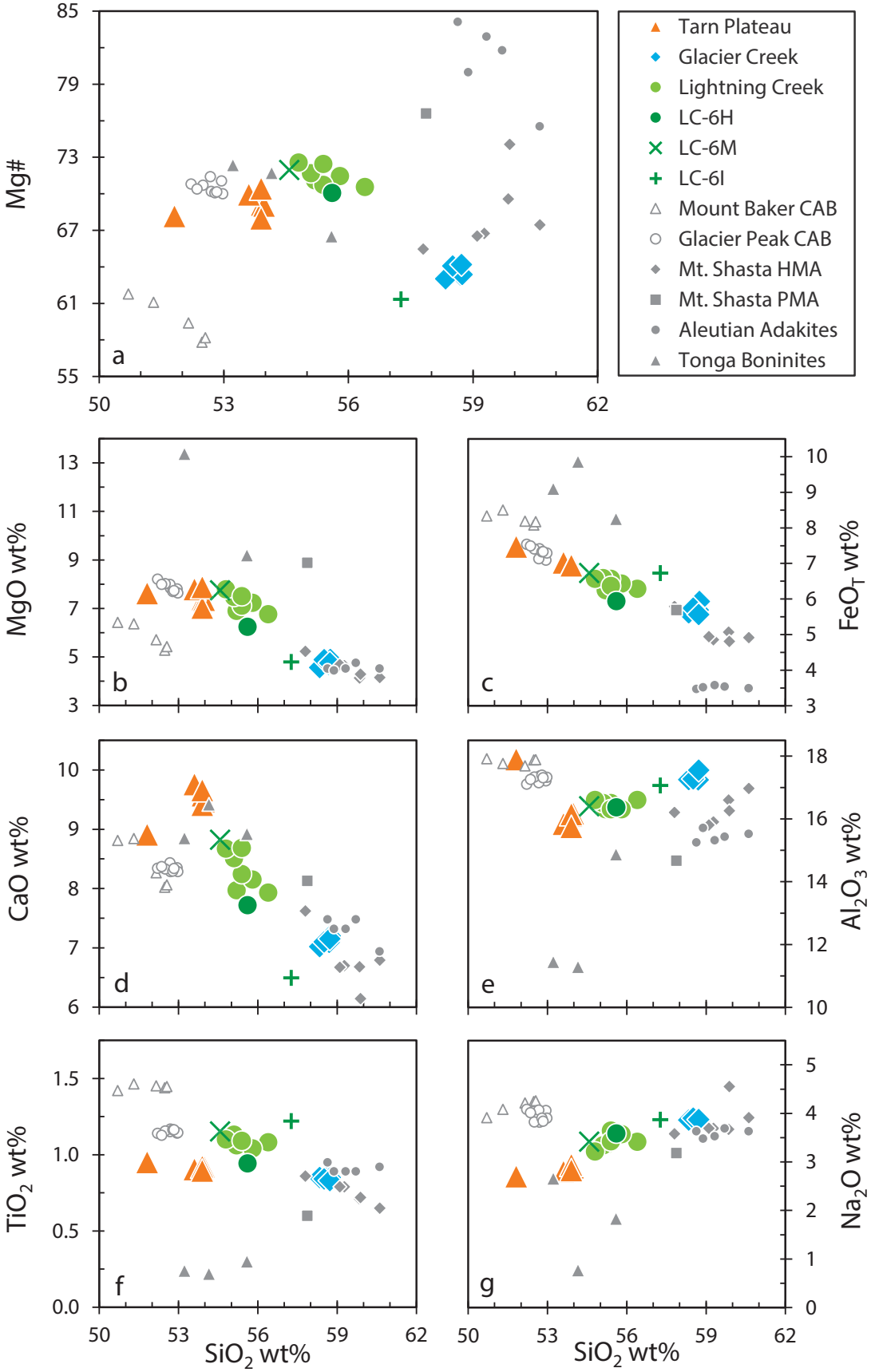
Tarn Plateau
Glacier Creek
Lightning Creek
LC-6H
LC-6M
LC-6I
Mount Baker CAB
Glacier Peak CAB
Mt. Shasta HMA
Mt. Shasta PMA
Aleutian Adakites
Tonga Boninites
Mg#
MgO wt%
FeO$_T$ wt%
CaO wt%
Al$_2$O$_3$ wt%
TiO$_2$ wt%
Na$_2$O wt%
SiO$_2$ wt%
a
b
c
d
e
f
g

Figure 6

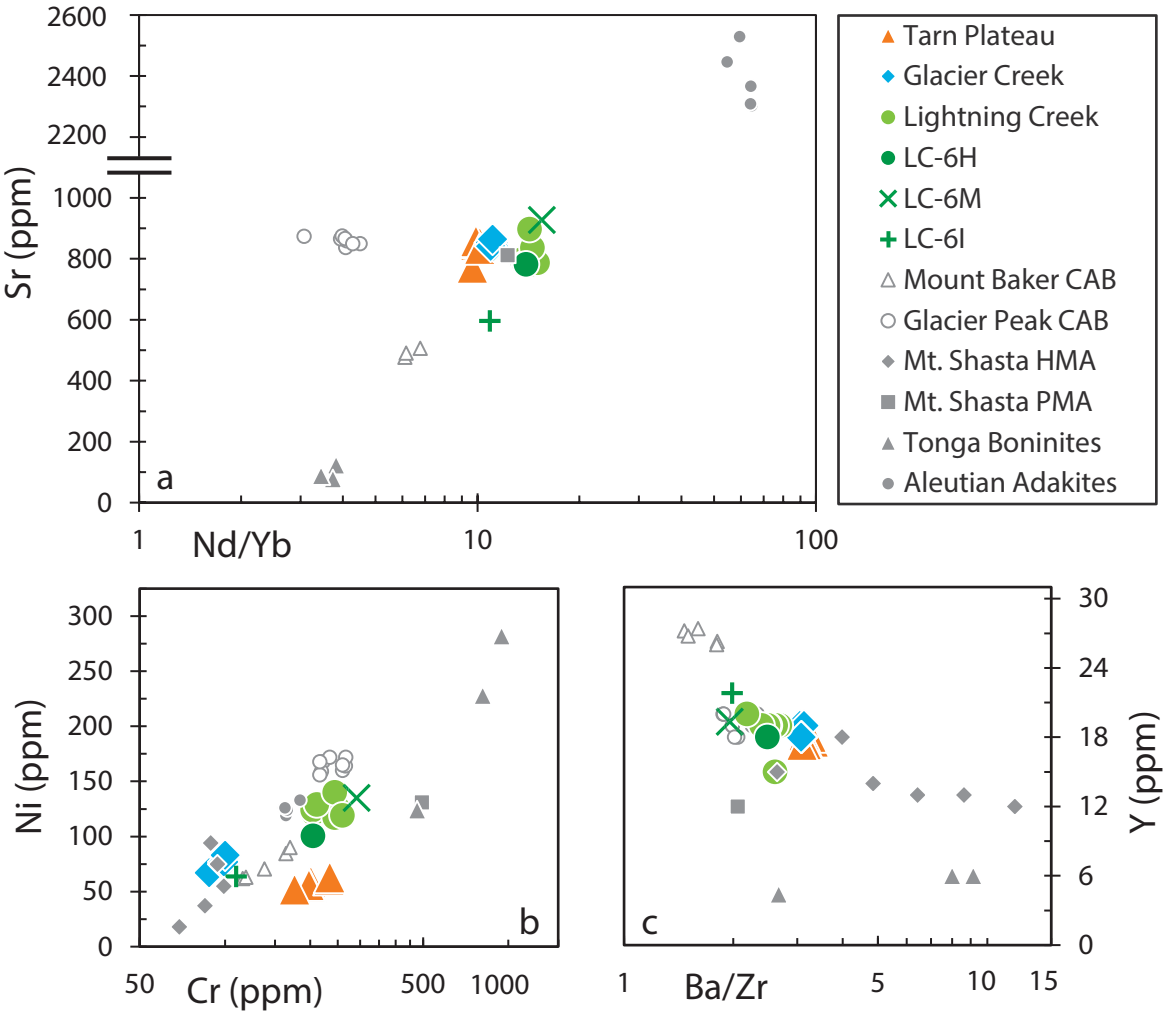
Sr (ppm)
2600
2400
2200
1000
800
600
400
200
0
a
1
Nd/Yb
10
100
Tarn Plateau
Glacier Creek
Lightning Creek
LC-6H
LC-6M
LC-6I
Mount Baker CAB
Glacier Peak CAB
Mt. Shasta HMA
Mt. Shasta PMA
Tonga Boninites
Aleutian Adakites
Ni (ppm)
300
250
200
150
100
50
0
b
50
Cr (ppm)
500
1000
c
1
Ba/Zr
5
10
15
Y (ppm)
30
24
18
12
6
0

Figure 7

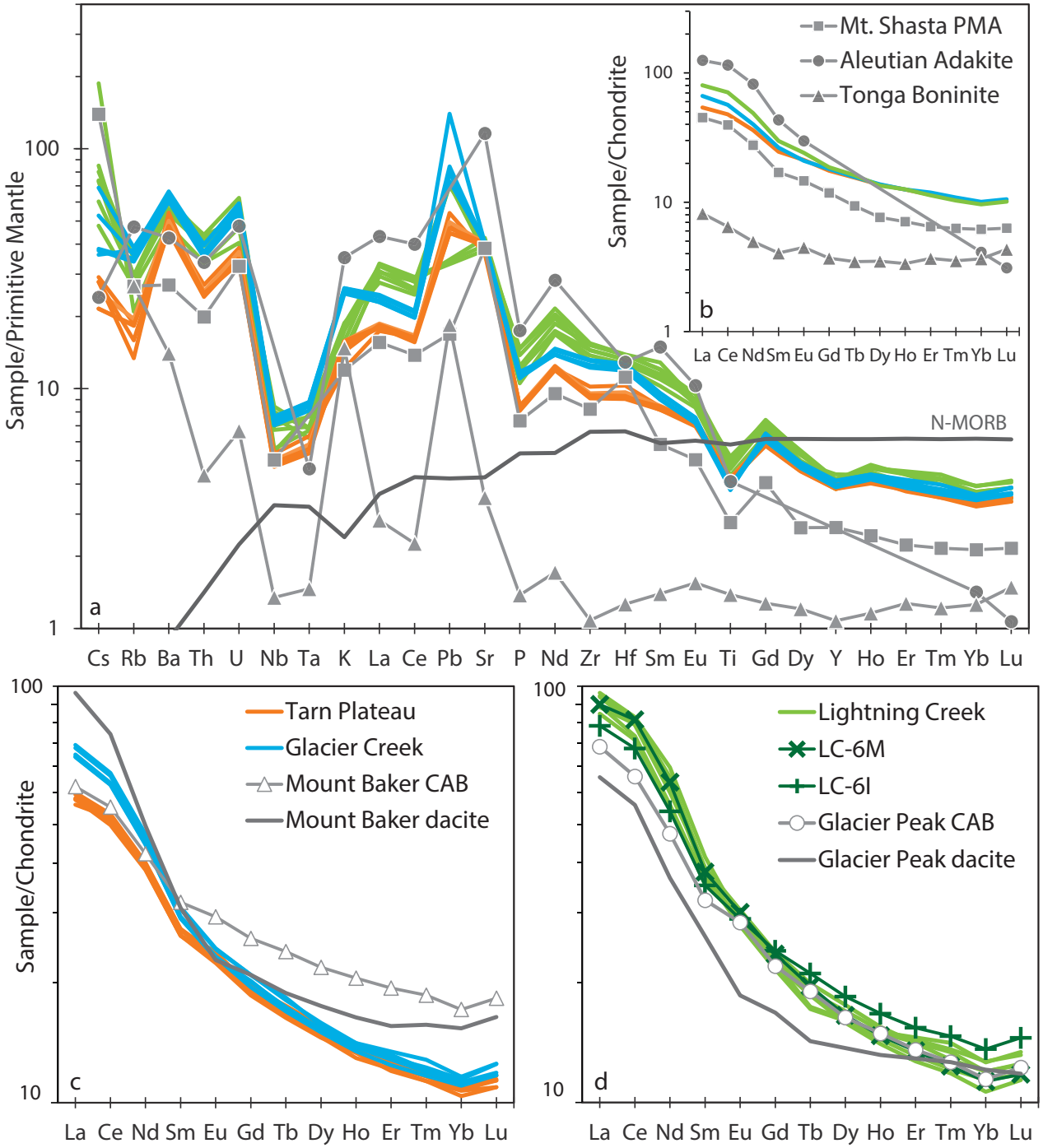
Sample/Primitive Mantle
100
10
1
a
Cs Rb Ba Th U Nb Ta K La Ce Pb Sr P Nd Zr Hf Sm Eu Ti Gd Dy Y Ho Er Tm Yb Lu
N-MORB
Sample/Chondrite
b
La Ce Nd Sm Eu Gd Tb Dy Ho Er Tm Yb Lu
Mt. Shasta PMA
Aleutian Adakite
Tonga Boninite
Tarn Plateau
Glacier Creek
Mount Baker CAB
Mount Baker dacite
c
Lightning Creek
LC-6M
LC-6I
Glacier Peak CAB
Glacier Peak dacite
d

Figure 8

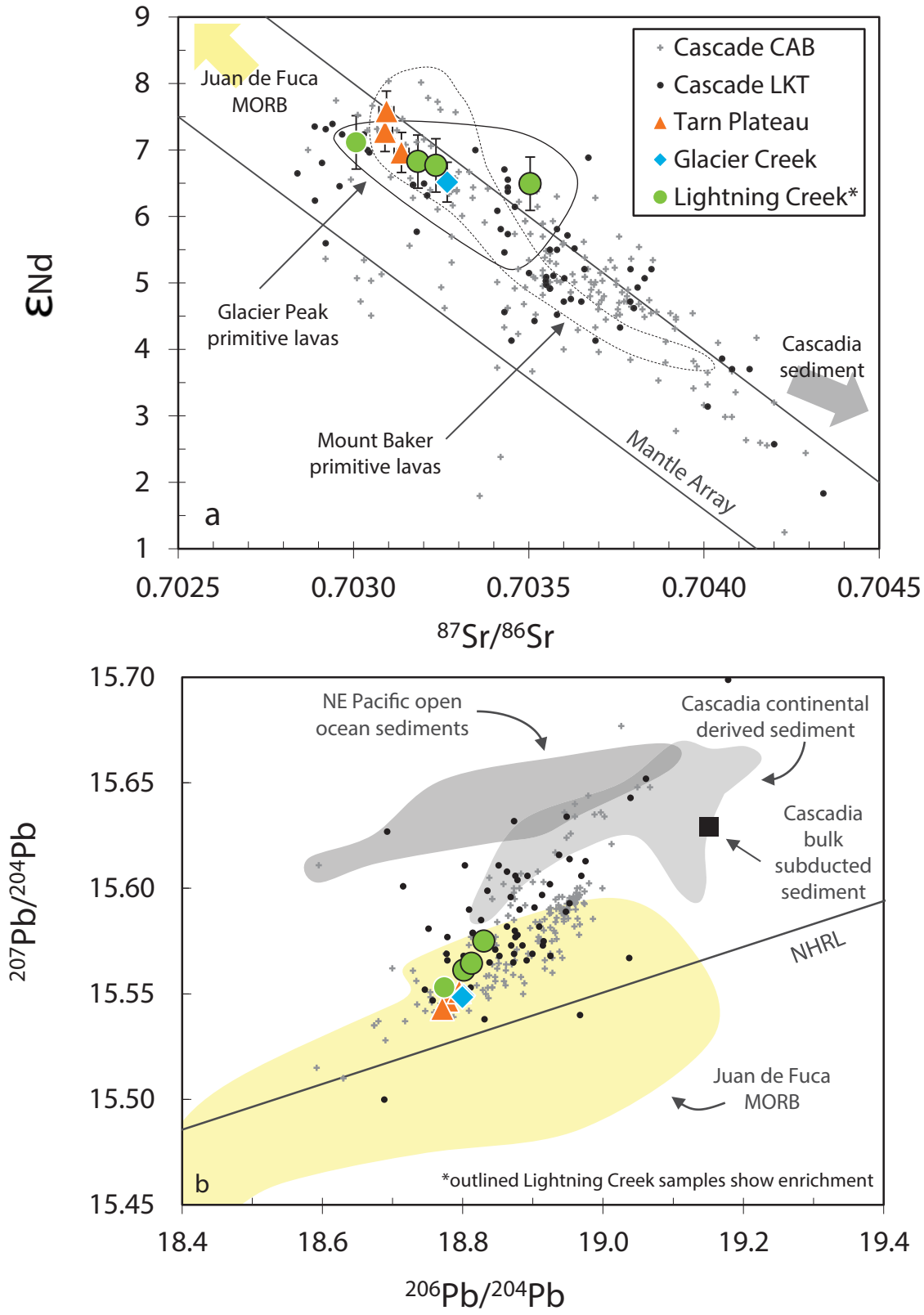
Cascade CAB
Cascade LKT
Tarn Plateau
Glacier Creek
Lightning Creek*
Juan de Fuca MORB
Glacier Peak primitive lavas
Mount Baker primitive lavas
Cascadia sediment
Mantle Array
a
εNd
87Sr/86Sr
NE Pacific open ocean sediments
Cascadia continental derived sediment
Cascadia bulk subducted sediment
NHRL
Juan de Fuca MORB
b
*outlined Lightning Creek samples show enrichment
207Pb/204Pb
206Pb/204Pb

Figure 9

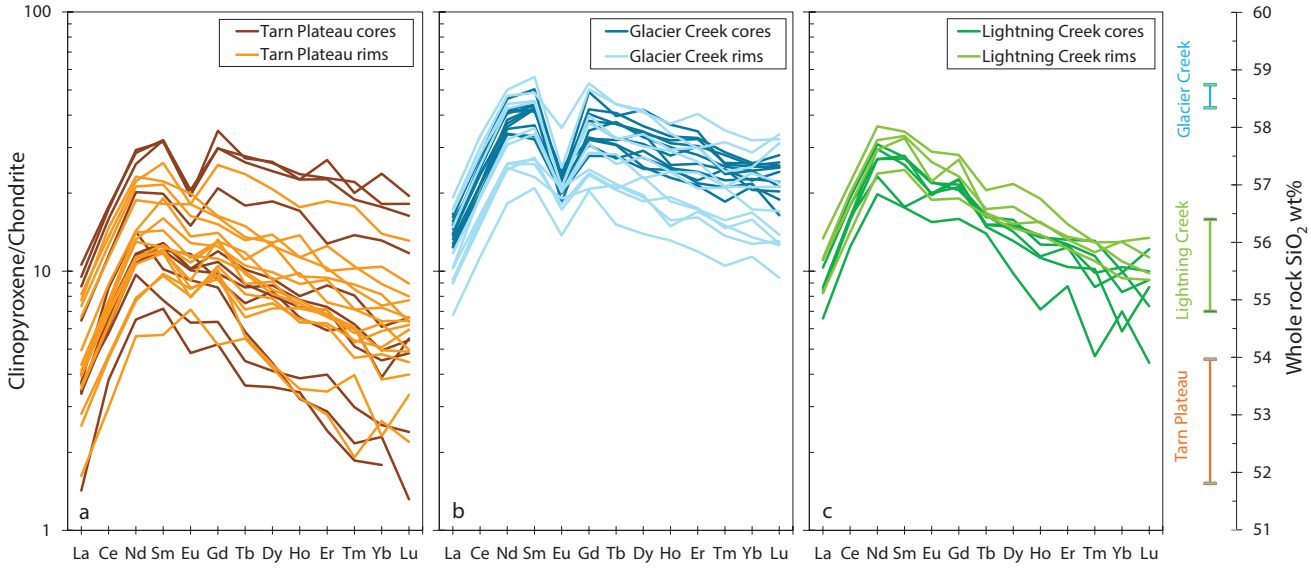


Figure 10

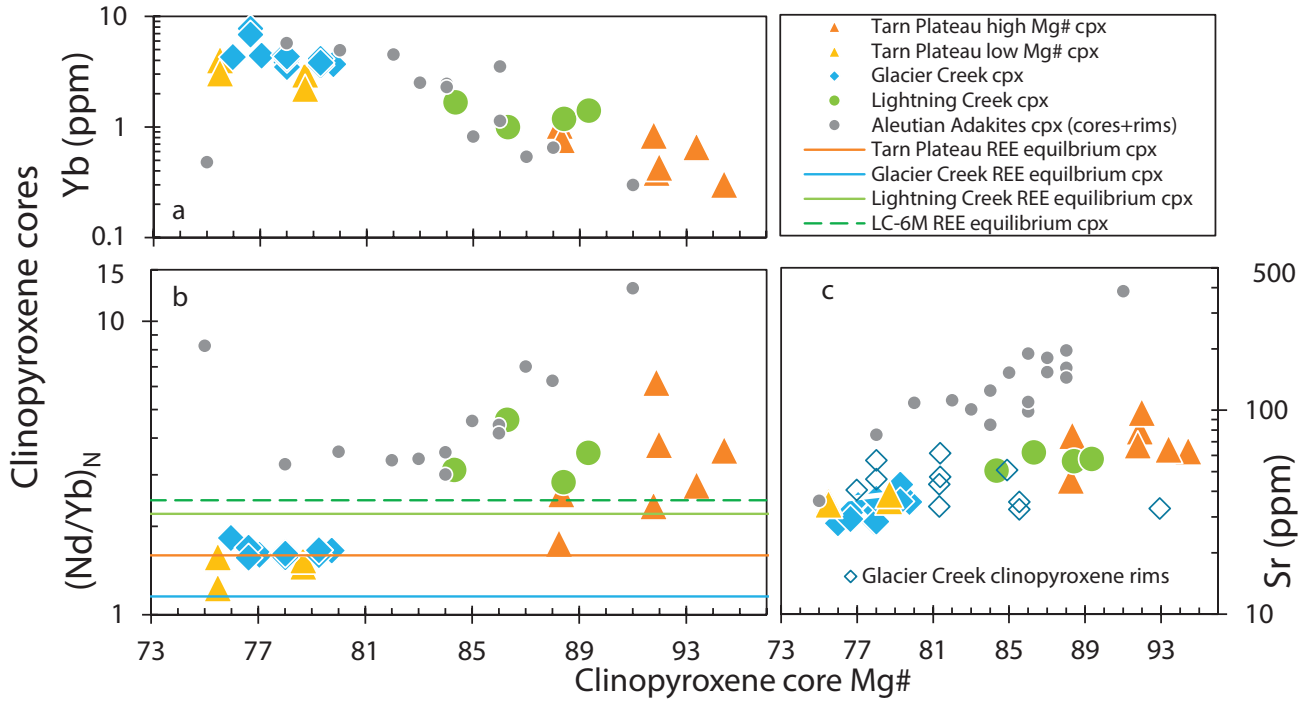
Clinopyroxene cores
Yb (ppm)
10
1
0.1
a
Tarn Plateau high Mg# cpx
Tarn Plateau low Mg# cpx
Glacier Creek cpx
Lightning Creek cpx
Aleutian Adakites cpx (cores+rims)
Tarn Plateau REE equilbrium cpx
Glacier Creek REE equilbrium cpx
Lightning Creek REE equilibrium cpx
LC-6M REE equilibrium cpx
(Nd/Yb)N
15
10
1
b
c
500
100
10
Sr (ppm)
Glacier Creek clinopyroxene rims
73
77
81
85
89
93
Clinopyroxene core Mg#

Figure 11

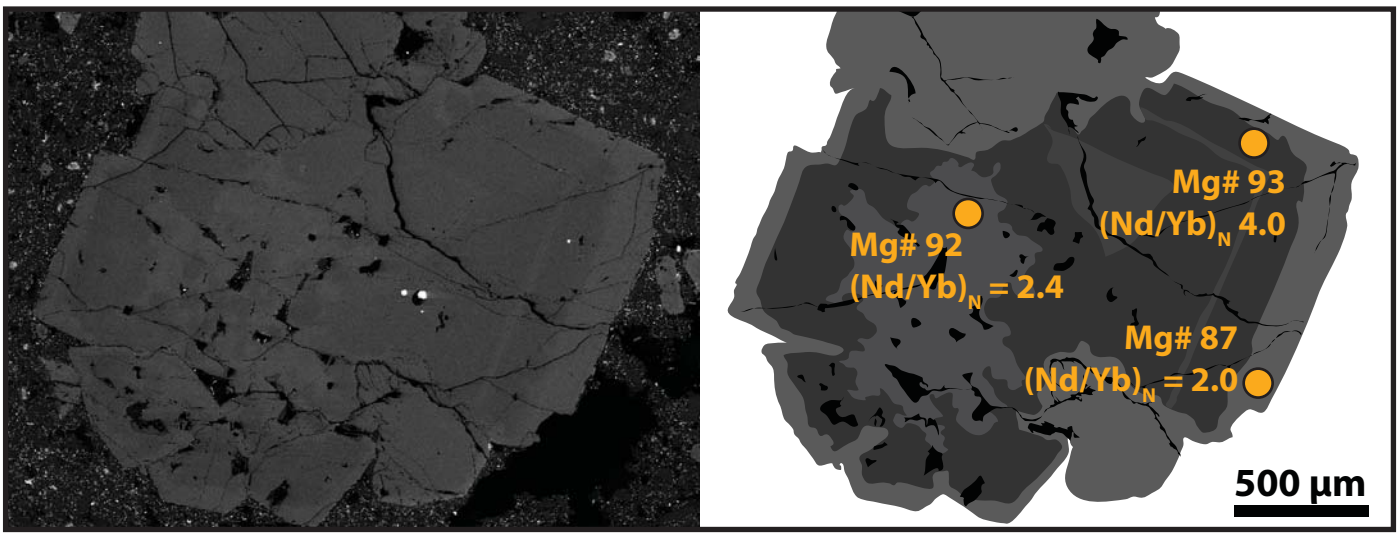


Figure 12

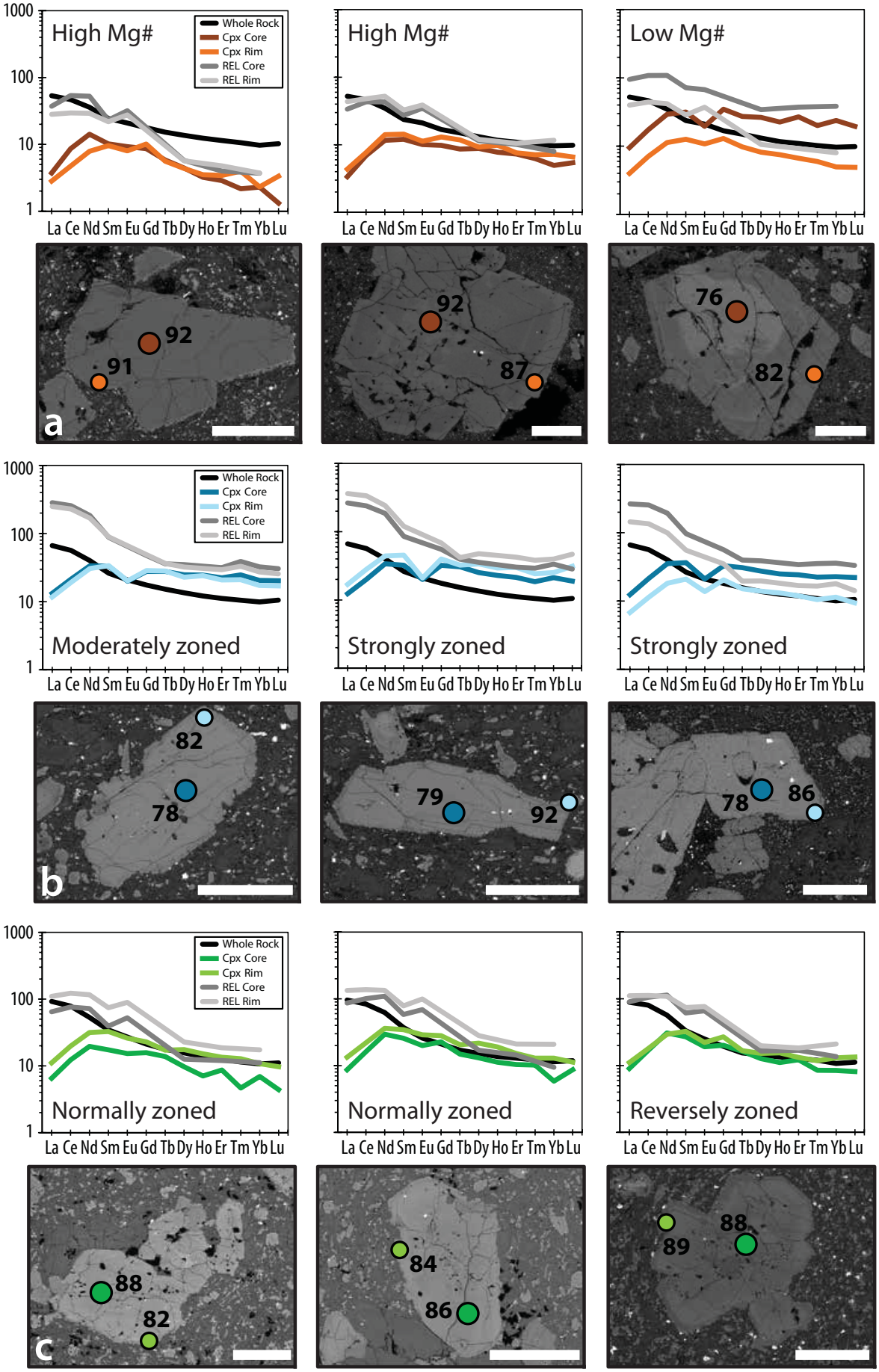
High Mg#
Whole Rock
Cpx Core
Cpx Rim
REL Core
REL Rim
High Mg#
Low Mg#
1000
100
10
1
La Ce Nd Sm Eu Gd Tb Dy Ho Er Tm Yb Lu
92
91
92
87
76
82
a
Moderately zoned
Strongly zoned
Strongly zoned
82
78
79
92
78
86
b
Normally zoned
Normally zoned
Reversely zoned
88
82
84
86
88
89
c

Figure 13

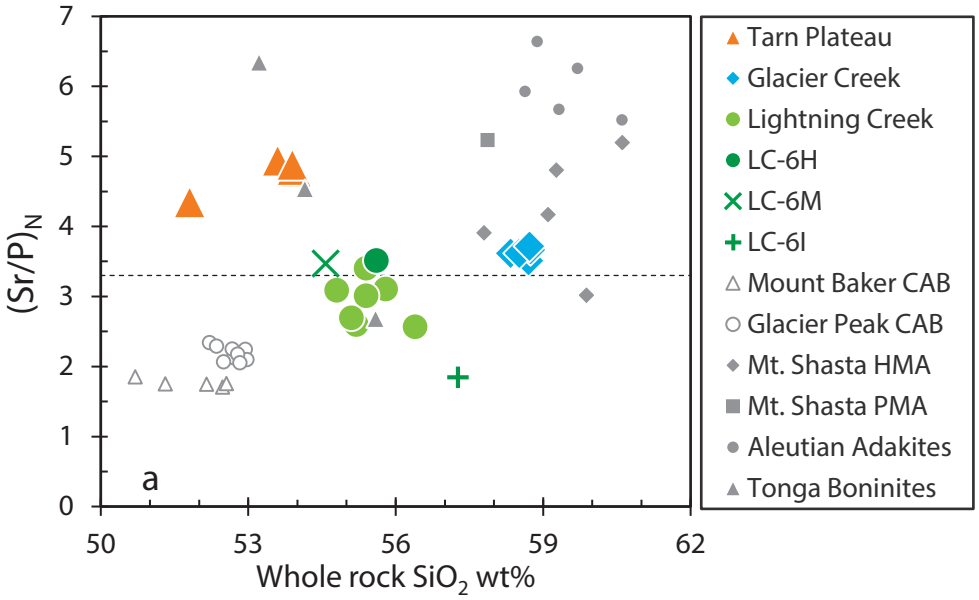
7
6
5
4
3
2
1
0
(Sr/P)N
a
50
53
56
59
62
Whole rock SiO2 wt%
Tarn Plateau
Glacier Creek
Lightning Creek
LC-6H
LC-6M
LC-6I
Mount Baker CAB
Glacier Peak CAB
Mt. Shasta HMA
Mt. Shasta PMA
Aleutian Adakites
Tonga Boninites

Figure 14

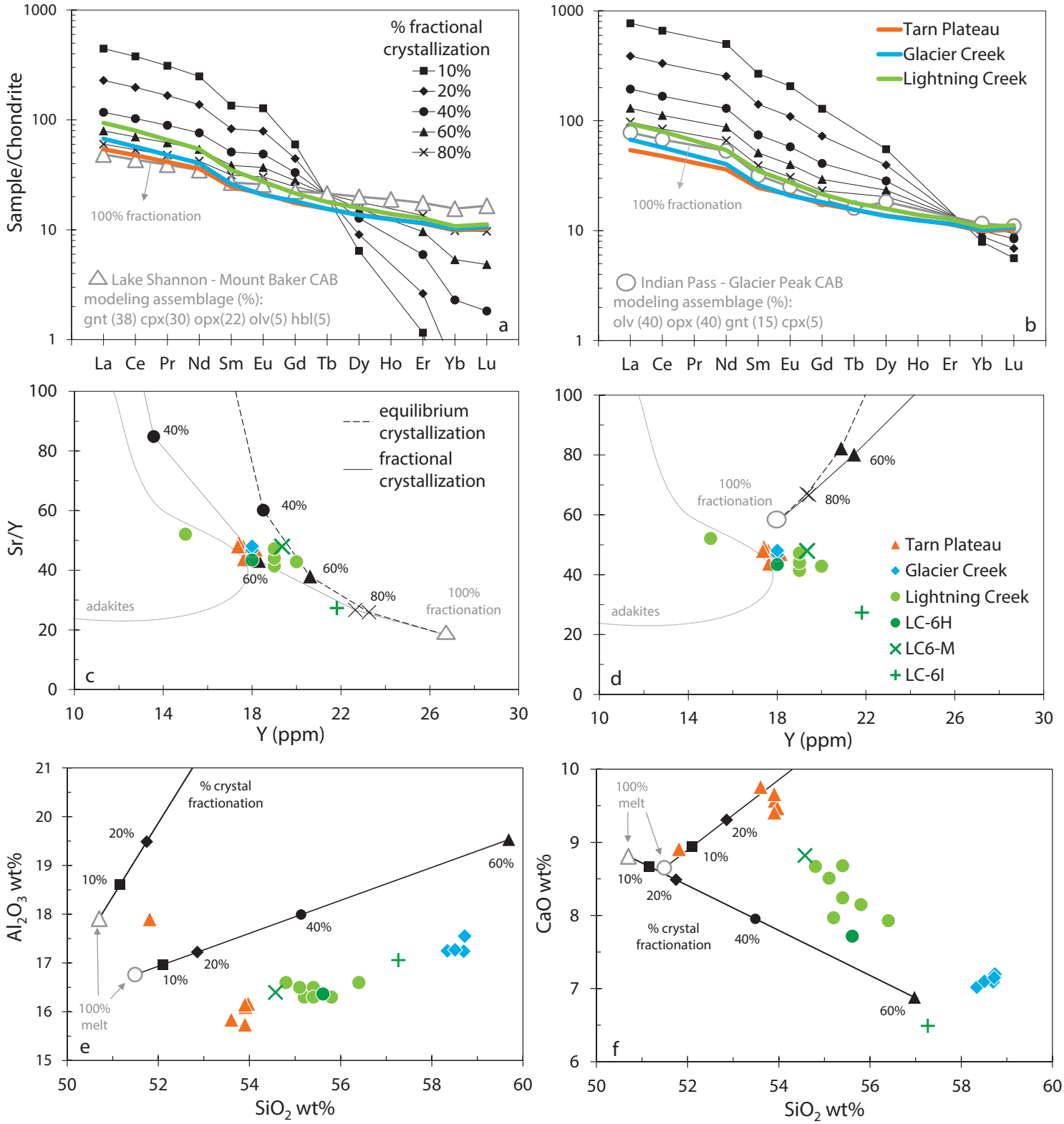
Sample/Chondrite
% fractional crystallization
10%
20%
40%
60%
80%
100% fractionation
Lake Shannon - Mount Baker CAB
modeling assemblage (%):
gnt (38) cpx(30) opx(22) olv(5) hbl(5)
a
Tarn Plateau
Glacier Creek
Lightning Creek
Indian Pass - Glacier Peak CAB
modeling assemblage (%):
olv (40) opx (40) gnt (15) cpx(5)
b
La Ce Pr Nd Sm Eu Gd Tb Dy Ho Er Yb Lu
Sr/Y
Y (ppm)
equilibrium crystallization
fractional crystallization
adakites
100% fractionation
c
d
Tarn Plateau
Glacier Creek
Lightning Creek
LC-6H
LC6-M
LC-6I
$Al_2O_3$ wt%
$SiO_2$ wt%
% crystal fractionation
100% melt
e
CaO wt%
f

Figure 15

This is a preprint, the final version is subject to change, of the American Mineralogist (MSA)
Cite as Authors (Year) Title. American Mineralogist, in press.
(DOI will not work until issue is live.) DOI: http://dx.doi.org/10.2138/am-2017-5756

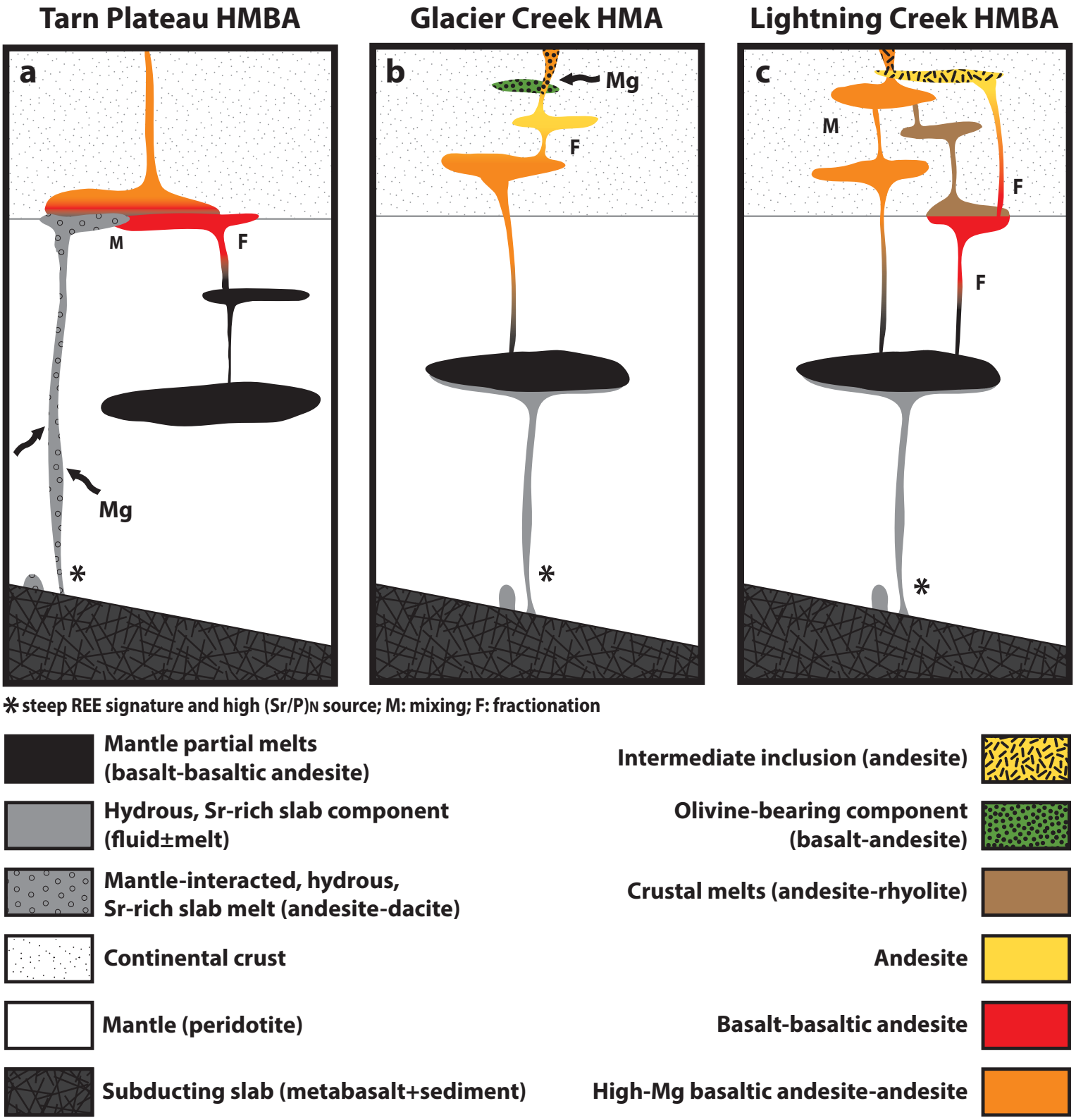


Figure 16